JOURNAL OF MATERIALS SCIENCE 29 (1994) 5232–5258

Review
Laser-beam and photon-assisted processed materials and their microstructures

J. SINGH
Applied Research Laboratory, P.O. Box 30. Penn State University, State College, PA 16804, USA

Laser processing is a relatively new technique for modifying the near-surface region of materials without altering the in-bulk characteristics. A single laser can perform several functions by manipulating processing conditions such as laser power, beam diameter, and traverse speed. Lasers have shown attractive applications, such as cutting, welding, glazing, alloying, and cladding. A laser glazing process has demonstrated an improvement in the microstructure of vacuum plasma-coated copper-based alloys containing cavities, unmelted particles, and segregation. Laser glazing has also been shown to restore the degraded microstructure of components and make them equivalent to, or better than, the original wrought alloy. The laser cladding concept was used to develop nickel-based alloys for high-temperature applications that exhibited higher thermal stability than the nickel-based Rene-95 alloy. Rapid melting and quenching occurred during the laser glazing, alloying, and cladding processes resulting in a fine-grained microstructure, metastable phases and extended solid solubility of alloying additions in the matrix.

Photon-assisted processing of material is a relatively new technique being explored to synthesize new materials from various substrates (solid, liquid, and gas). This process is successfully used to fabricate high-quality thin films for electronic industries. Thin films of multicomponents can be deposited with stoichiometric composition. Diamond thin films have been synthesized from liquid hydrocarbon (Benzene, C_6H_6) by laser–liquid hydrocarbon–substrate interaction. A laser-assisted physical vapour deposition process was found to be very successful in depositing stoichiometric compositions of multilayered thin films such as superconducting $YBa_2Cu_3O_7$, ferroelectric $Pb_{0.52}Zr_{0.48}TiO_3$ and other coatings such as TiN and $CoSi_2$. This review reports some of the major advances in the understanding and engineering of new materials for electronic industries and high-temperature applications in the auto, aerospace, and turbine industries.

1. Introduction

The laser, as a source of "pure" energy in the form of monochromatic and coherent photons, is enjoying ever increasing popularity in diverse and broad applications from eye surgery, to drilling micrometre-sized holes on semiconductor devices, to guidance systems used in drilling a mammoth tunnel under the English Channel. It has become a valuable tool in areas such as metallurgy, medical technology, and the electronics industry.

Like many other discoveries, various applications of the laser were not initially defined, but were a consequence of natural evolution led by theoretical studies. Shortly after the exploratory demonstration of the first laser (early in the 1960s), most intensive theoretical studies dealt with laser beam–solid interaction. Experiments were undertaken to verify different theoretical models for this process. Later, these experiments became the pillar of many applications. Fig. 1 illustrates the history of laser development from its initial discovery to practical applications. In recent years, the branches of this tree have started to bloom and bear fruit. Laser processing of materials is only a small branch of the growing tree.

The objective of this paper is to provide an overview of laser technology and applications which can serve as a starting point for those who are interested in implementing or modifying the existing process or to building upon past work to develop new applications. Before proceeding further, four questions need to be answered.

1. What is a laser ?
2. What is the physics of laser beam-solid interaction ?
3. What is the applications of laser in the materials area ?
4. What is the effect on microstructure and properties of materials ?

0022–2461

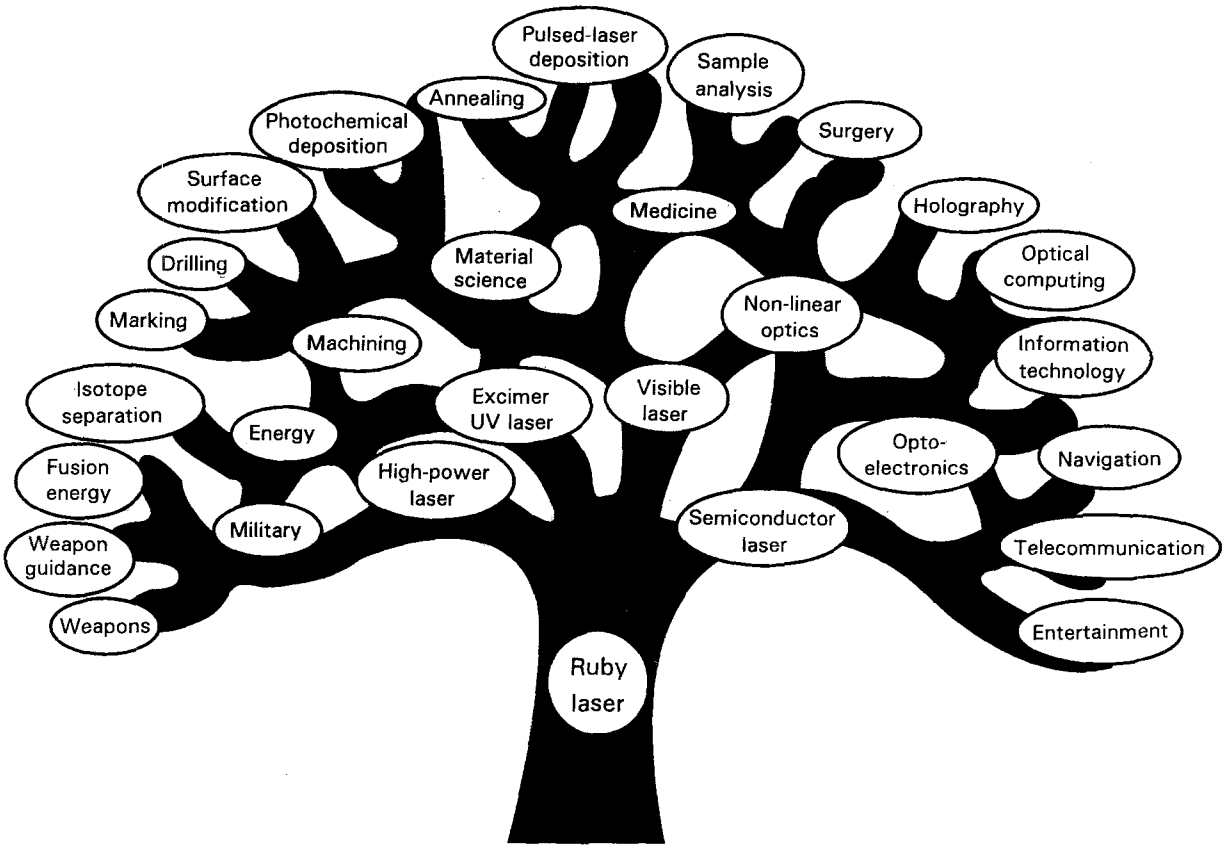

Figure 1 Evolution of laser technology and its applications [1].

2. Laser theory

The term laser stands for Light Amplification by Stimulated Emission of Radiation. It is necessary, first, to know the origin of laser light. Light may be modelled either as an electromagnetic wave or as discrete particles with a certain amount of energy associated with it, depending on its wavelength. Light is generated by the displacement or oscillation of electric charges. Consider a single atom or molecule surrounded by an electron having specific energy, E_1 (Fig. 2a). When an incoming photon of appropriate energy collides with the atom, it is absorbed and an electron in orbit around the nucleus is raised to a higher energy level, E_2 (i.e. larger orbit) corresponding to the energy of the photon (Fig. 2b).

If sufficient time is given, the excited electron, E_2, will return to its original state, E_1, by the releasing the same amount of absorbed photon energy (Fig. 2c). The wavelength of the photon released is determined by the energy involved in the transition and is given by

$$E_2 - E_1 = h\,(c/\lambda) = h\nu \qquad (1)$$

where h is Planks constant $= 6.6256 \times 10^{-34}$ (J s); c the speed of light in a vacuum $= 2.99 \times 10^8$ (m s^{-1}); ν is the laser frequency, and λ the wavelength of light (metres). If the energy of the photon (incoming) does not correspond to the energy difference between the two orbits (i.e. $h\nu \neq E_2 - E_1$), the absorption process will not occur.

Let us consider an atom in the excited state which collides with a photon equal in energy to the difference between the upper and lower energy levels (Fig. 2d). When this occurs, two photons are present after the collision and the atom has returned to the lower energy state. The two photons have the same wavelength, are travelling in the same direction as the incoming photon, and are in phase. As in the case with absorption, the energy of each photon must be equal to the energy difference between the upper and lower energy states. Such a lasing action is referred to as a stimulated emission process.

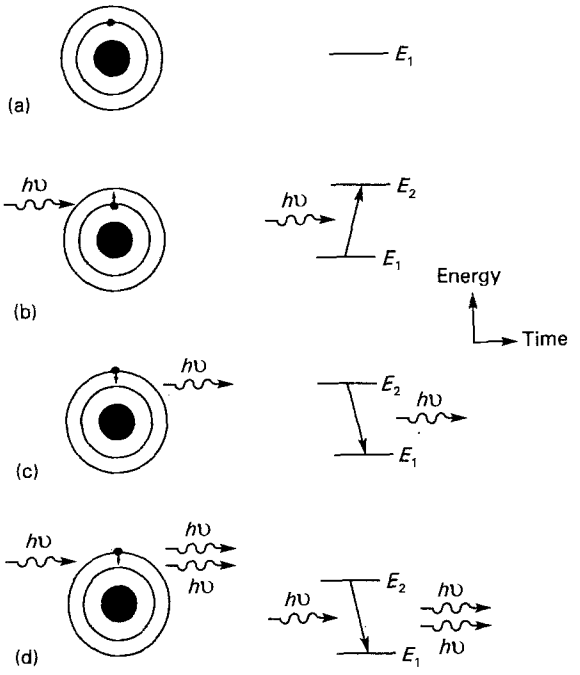

Figure 2 Atomic absorption and radiation.

The above situation can be created on a large scale by introducing a gas (for example, CO_2 gas laser) at sub-atmospheric pressure in a confined glass tube containing two electrodes and two mirrors, as shown in Fig. 3a. The function of the mirrors will be discussed in the next section. When power is applied to the electrodes, current is passed through the gas. The current flow causes electrons to collide with the gas molecules. This causes the electrons in the gas molecule to be excited to a higher energy level (e.g. larger orbit according to the classical interpretation). This collision process supplies the energy for the laser action to take place. This process can be considered to occur in three steps as shown in Fig 3. The first step results from spontaneous emission. Spontaneous emission is simply the quantity of light (photon) released when an excited molecule decays to a lower energy state, referred to as the lower laser level. When spontaneous emission occurs, photons are released in all directions (step one, Fig 3a). Some of the photons travel along the axis of the laser and collide with molecules which are in the upper level. When this occurs, an additional photon is released travelling in the same direction with the same wavelength and phase as the photon that collided with the excited molecule (step two, Fig 3b). This process is known as stimulated emission, i.e. a photon stimulates an excited molecule to emit a second photon. Many of these collisions occur, and the intensity of the light builds or becomes amplified within the laser cavity. Thus, the process is termed amplification (step three, Fig 3c).

The function of the mirrors in the laser is two-fold. First, mirrors simply direct the photons back into the laser cavity (also called glass tube) to increase further the intensity of the light. Second, and less obvious, the mirrors control the exact wavelength of the laser light. When spontaneous emission occurs, all of the light released is not of the same wavelength, because both the upper and lower lying states have a bandwidth associated with them. In addition, the kinetic energy distribution of the emitting molecules, resulting from thermal agitation and collision, is also very important in determining the wavelength variation of the emitted photons. The mirrors have the effect of limiting the wavelength variation of the laser light by supplying boundary conditions, which allow only certain wavelengths to build up in the cavity. This phenomenon, known as optical resonance, is analogous to that of an organ pipe which resonates only at frequencies where the pipe length divided by the sound wavelength is an integer (or an integer plus 1/2, depending on the end condition of the light). For the laser cavity to resonate, the wave must fit into the space between the mirrors, just as the sound waves must fit into the organ pipe. All other wavelengths will die out as a result of destructive interference at the mirrors. For two flat mirrors, the condition for resonance is

$$n\lambda = 2d \qquad (2)$$

where $n = 1, 2, 3, \ldots$: λ is the wavelength (metres): and d the distance between mirrors (metres).

The primary parts of a laser and its basic operating principles have been discussed above. Now, a laser can be visualized as being comprised of four parts:

1. the Medium, in which the energy conversion takes place;
2. the Optical resonator (mirrors), which provides feedback into the gain medium and controls the exact wavelength of the light output;
3. the Power source, which conditions the flow into the laser; and
4. Cooling system, which removes the waste heat from the lasing medium and the resonator (glass tube).

The wavelength of the laser depends upon the glazing medium in which energy conversion takes place. There are two types of glazing media: the solid laser (Nd:YAG laser) and the gas laser (CO_2, argon-ion, KrF). The Nd:YAG is a solid-state laser consisting of a yttrium aluminium garnet crystal doped with neodymium. The krypton fluoride (KrF) laser is also called an excimer laser or gas halide laser. There are roughly 30 types of commercially available lasers. Details of each laser (i.e. wavelength, mode of operation, power) and their typical applications are given in Table I.

Processing of materials by a laser-beam depends on the absorption of the laser beam energy directly or indirectly on the work piece. Direct laser-beam processing of materials has a wide range of applications such as cutting, welding, and cladding. In the indirect laser-beam processing of materials, high-energy photons do not directly interact with the work piece or substrate. In fact, the laser beam is used to interact with the target (which can be solid, liquid or gas) and the product is collected on the work piece for its potential applications. That is why this process is

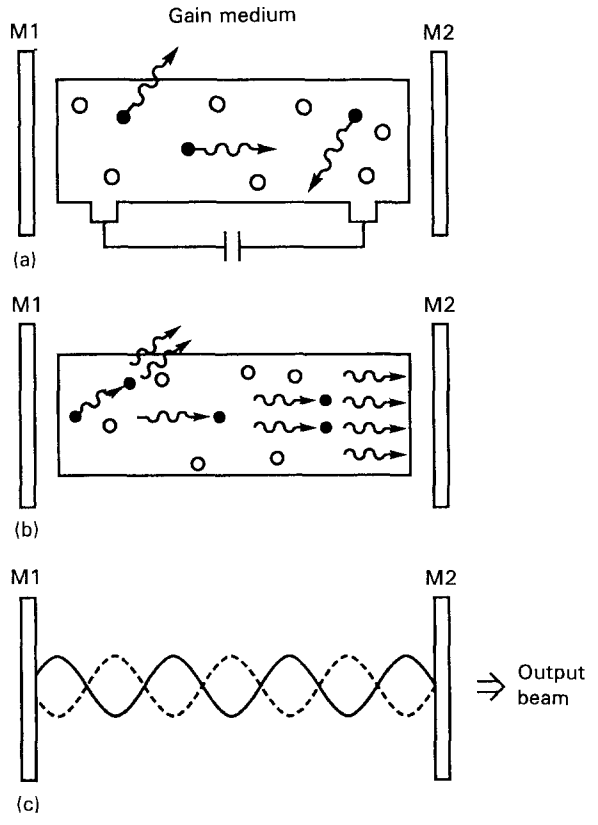

Figure 3 Buildup of light in laser cavity.

TABLE I Types of laser and their applications

Laser	Wavelength (μm)	Mode of typical operation	Power (W)	Typical applications
CO_2	10.6	CW	10000 (10 KW)	Heat treating, welding, cutting cladding
		Pulsed	1000	Welding, material removal
Nd:YAG	1.06	CW	300	Welding
		Pulse	5000	Trimming
		(Q-switched) Pulse	200	Welding, hole drilling
Ruby	0.6943	Pulsed	10^5	Spot welding, hole drilling
Nd:Glass	1.06	Pulsed	10^6	Spot welding, hole drilling
Argon	0.4880			
	0.5145	CW	20	Semiconductor
KrF	0.248	Pulsed	100	Semiconductor, material removal

called photon-assisted processing of materials. Laser-assisted physical vapour deposition (LAPVD) or chemical vapour deposition (LACVD) are the typical examples which fall under this category. The physics of direct-beam processing of materials will be discussed next, followed by the physics of indirect beam (i.e. photon-assisted) processing of materials.

3. Physics of direct laser-solid interaction

The interaction of the laser beam, i.e. photons, with the matter occurs primarily by electronic excitations. Electrons absorb quanta of light energy and are raised to higher energy states. The excited electrons collide with the lattice atoms and transfer the energy to the lattice in the form of photons in a time of the order of 10^{-12} s or less. The electrons very rapidly give up their energy in collisions in a time of the order of 10^{-12} s or less. The energy is thus transformed very rapidly into lattice vibrations, i.e. into heat. The amount of heat generated at the surface of material will create two extreme conditions, i.e. laser-induced surface heating and melting. A brief description and conditions governing each of these cases will be discussed below.

In the laser-induced surface heating model where the heating cycle is very short (of the order of few picoseconds), beam dimensions are also in general quite small as compared to the black body substrate, and assuming there is no energy loss from convective current in the surroundings, the temperature distribution, $T(x, y, z, t)$, along the z-axis in the sample surface can be described by

$$dT/dt = Q/\rho c_p + d(D dT/dz) \quad (3)$$

where Q is the source term arising from the laser beam having been absorbed within the material, and D, the thermal diffusivity, is given by $D = K/c_p\rho$. In general, Q is defined as

$$Q = I(r,t)(1 - R)F(z) \quad (4)$$

where $I(r,t)$ is the incident beam intensity, R is the sample reflectivity, and $F(z)$ is a function that expresses the penetration depth of the laser light in the material, while K, c_p and ρ represent the thermal conductivity, specific heat and density, respectively. If we assume that the workpiece is semi-infinite, all constants are independent of temperature, the target is a homogeneously absorbing medium, the absorption or penetration of laser light, Q, into the surface of conducting materials (such as metals) is described by the equation

$$Q(z) = I_0 (1 - R) \exp(\alpha Z) \quad (5)$$

where $Q(z)$ is the intensity of the light (laser energy) penetrating to depth z in the material, I_0 is the output laser power density at the surface ($W m^{-2}$), and α is the absorption coefficient of the material.

The laser, with proper wavelength, can be chosen so that the maximum absorption takes place within a small zone near the surface. The boundary conditions for the heat flux depend upon the intensity profile of the laser beam (i.e. beam-energy distribution can be gaussian or doughnut shaped), spot size, the interaction time of the laser beam with the surface (i.e. traverse speed of the laser beam with respect to the substrate), and absorption coefficient. The absorption coefficient may depend not only on the wavelength of the laser light and type of material, but also upon the surface finish and surface temperature. For metals, the absorption coefficient is typically in the range 10^4–10^5 cm^{-1}. Generally speaking, for a clean metal surface, the absorption increases as the temperature is increased and absorption is generally larger at shorter wavelength.

For surface modification processes, in which there is no phase change, the maximum temperature rise at the surface during the irradiation process is given by

$$T_s = (I_0/K)(4kt/\pi)^{1/2} \quad (6)$$

where, K is the thermal conductivity of the material ($W cm^{-2}$), k thermal diffusivity ($cm^2 s^{-1}$), and t the time of laser-beam interaction with the material.

After the energy is absorbed, it is transformed through the material by thermal conduction. When there is no phase change in the material, then the depth, z, of penetration of the heat energy in time is given by

$$z = (4kt)^{1/2} \quad (7)$$

where k is the thermal diffusivity of the material.

If the laser flux is increased to above the melting point of the material (i.e. there is a phase change), then the above equations are not valid. Other complex physical phenomena come into operation, such as melting and/or vapourization. The vapourized material absorbs some of the incident laser light and becomes

heated and ionized. Collection of the vaporized product is often called photon-assisted processing of materials. The physics of hot-ionized plasma formation at the laser-solid interaction will be discussed first, followed by substrate surface melting in the next sections.

4. Photon-assisted processing of materials

Photon-assisted processing of materials from vapour, gas or liquid environments fall into this category. Each process has its own merits and limitations. The synthesis of material from the liquid phase is the most recent and this novel techniques is still being explored. The physics of each process will be discussed below, together with their applications.

4.1. Laser-assisted physical vapour deposition

Laser-induced vapourization of materials has been known for a long time, although its utilization for thin-film synthesis is very recent. This process is often called laser-assisted physical vapour deposition (LAPVD) which is one of the small branches of the tree (Fig. 1). It is used for high-quality thin-film deposition in micro-electronic industries. In this process, a pulse laser beam is used to vapourize materials (target) in a vacuum chamber (at a pressure of $\sim 10^{-6}$ torr, 1 torr = 133.322 Pa) and the evaporant is collected or deposited in the form of a thin film on a substrate. Thin film is deposited at a rate of a few tenths of a nanometre per pulse. The LAPVD is probably the simplest among all thin-film growth techniques. Fig. 4 shows a schematic diagram of this technique.

The beam–solid interaction is wavelength dependent. Because lasers are available in a broad spectrum of wavelengths, pulse energies, and pulse widths, it is envisioned that with the choice of appropriate laser, LAPVD deposition can be used to deposit thin films of almost any material. The versatility of this technique is reflected in the fact that almost 128 different materials have been deposited in thin-film form by LAPVD [2].

4.2. Physics of the LAPVD technique

Although LAPVD is an extremely simple technique, the beam–solid interaction that leads to evaporation/ablation is a very complex physical phenomenon. The LAPVD process involves four steps which can be illustrated with the help of Fig. 5. A laser beam hits the surface of a solid target material, electromagnetic energy (photon) is converted into electronic excitation and then into thermal energy (step I) to cause molten layer formation (step II), ablation and then evaporation (step III), excitation, expansion of evaporant and plasma formation (step IV). Each of the four regimes is discussed separately below.

4.2.1. Laser-target interaction

Fig. 5b and c show schematic diagrams of the interaction of a laser beam with a solid target. Part of the

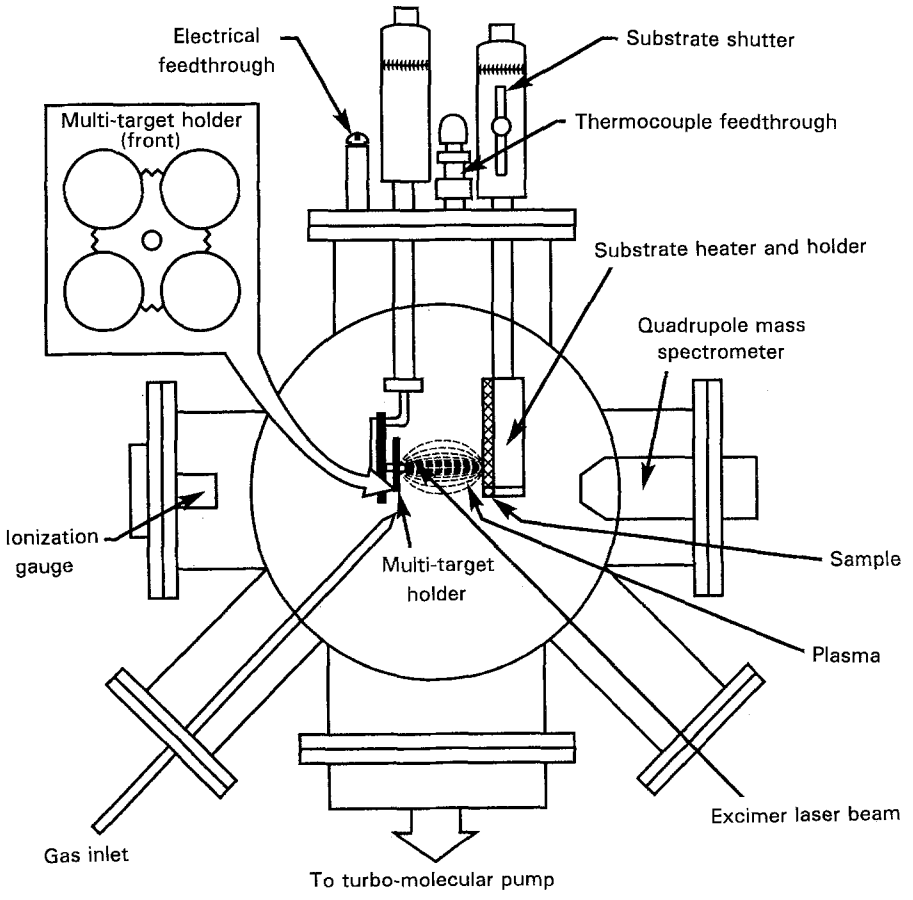

Figure 4 Schematic representation of laser-assisted physical vapour deposition system.

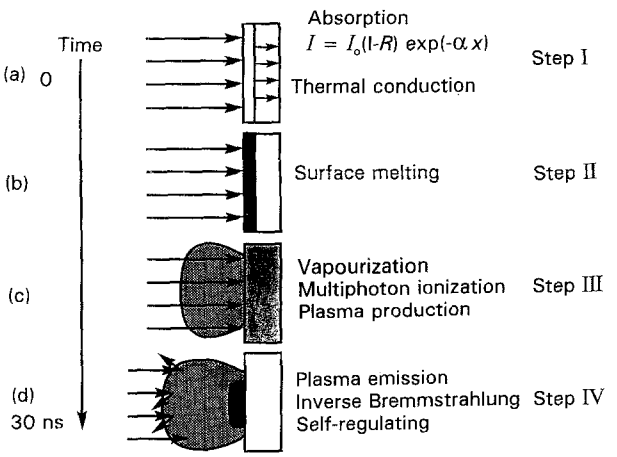

Figure 5 Schematic representation of the laser–target interaction.

beam is reflected, while the remainder is absorbed over a characteristic absorption depth given by α, where α is the absorption coefficient of the target. This value depends strongly on the wave of the incident laser beam and the band structure of the target material. The photon energy from the laser is transferred into the lattice (heat) in very short times (10^{-12} s). In nanosecond time scales, the heat diffusion distance in that target is in the range 50–500 nm. Thus, only the near surface of the target is rapidly heated and evaporated, which leads to stoichiometric evaporation of the material from the target.

4.2.2. Laser–evaporated material interaction

The evaporating material is further heated by the incoming laser radiation beam, resulting in the formation of a high-temperature, partially ionized plasma. The primary laser absorption occurs by an inverse Bremmstrahlung process which involves absorption of the photon by a free electron scattering in the presence of ions. Plasma–laser interaction results in further heating of the plasma and regulates further interaction of the radiation field with the target [3]. The absorption coefficient of the plasma, α, can be expressed as [4]

$$\alpha = 3.69 \times 10^8 \{Z^3 n_i^2 / T^{0.5} \nu^3 [1 - \exp(-h\nu/kT)]\} \quad (8)$$

Absorption radiation by the plasma is a function of the plasma density, n_i, the laser frequency, ν, and the plasma temperature, T. Z is the average charge. K is Boltzmann's constant and h is Plank's constant.

The term $[1 - \exp(-h\nu/kT)]$ represents the losses due to stimulated emission. If we consider an excimer laser (wavelength, $\lambda = 308$ nm), the exponential term becomes unity for $T \ll 40000$ K and can be approximated by $h\nu/kT$ for $T \gg 40000$ K. This absorption term shows a $T^{-0.5}$ dependence for low temperatures ($T \ll 40000$ K for $\lambda = 308$ nm, $T \ll 10000$ K for $\lambda = 1.06$ μm) and $T^{-1.5}$ for high temperatures. This dependence is an important factor in estimating the effect of energy density on the deposition characteristics. The heating of the evaporated material is controlled by the plasma absorption coefficient, which depends on the concentration of the ionized species, plasma temperature, wavelength, pulse duration, etc. The particle density in the plasma in turn depends on the degree of ionization, evaporation rate, and the plasma expansion velocities.

Heating by the laser beam is more efficient using longer wavelength laser and higher ionized plasmas. However, for shorter laser wavelengths, the ionization efficiency of the laser beam is much higher, primarily due to direct photoionization and coupled photothermal excitation/ionization mechanisms. Thus, shorter wavelength lasers are better in production of more ionized and high-temperature plasmas. The ionization efficiency is critical in determining the nature of vapour transport and the maximum transitional temperature of the plasma.

4.2.3. Adiabatic plasma expansion and deposition of thin films

The laser–target–plasma interaction is extremely complex due to the interdependent nature of the plasma absorption on the number of species present, wavelength, the fraction of ionized material, and the length of the pulse. Once the plasma is generated at the target surface, the plasma expands away from the target surface and the electron density decreases. Then, there is secondary interaction between the laser beam and the evaporants. Higher order interaction between the laser beam–evaporants indeed significantly affects the evaporants characteristics and plasma properties. Isothermal expansion of the plasma occurs during the laser interaction and is followed by an adiabatic expansion after the pulse ends. For sufficiently long pulses, the laser can interact again with the target, i.e. the initially formed plasma can be opaque to the laser radiation. As the expanding plasma moves away from the target and electron density decreases, the plasma can be transparent. In this way, the behaviour of plasma self-regulates the laser–target interaction. This is one of the reasons that a pulsed laser is used in this process.

The laser plume consists of neutral and ionized atoms and molecules, and particles clusters ejected from the target material. The kinetic energy of the ablated species from the target (e.g. $YBa_2Cu_7O_{7-\delta}$) has been measured by different groups and varies in the range 10 – 400 eV which are two to three orders of magnitude greater than the thermal energies [1,4]. The kinetic energy of the evaporant product is important for producing a high-quality thin film on the substrate. Therefore, it is important to understand the physics of plume or plasma dynamics.

Another important parameter in plasma dynamics is the velocity distribution of each species (i.e. time of flight of each species), especially when species are moving from the target to the substrate and when there is thermal distribution within the plasma. The relatively high velocities of the ionic species are $> 10^6$ cm s^{-1} for all energy densities, which corresponds to kinetic energies greater than 1 eV per nucleon. The high kinetic energy of the species has been explained by the rapid transformation of the thermal energy of the plasma during expansion in vacuum. From gas

dynamics, the maximum terminal velocity for one-dimensional expansion of plasma is

$$2(VRT)^{0.5}/V(M)^{0.5} \quad (9)$$

where V is the ratio of specific heat of plasma species, and M and T are the molecular weight and temperature of the plasma, respectively [1]. It has been speculated that the value of V for monatomic ionized high-temperature gas is in the range 1.3–1.4, instead of the thermodynamic value of 1.66. This results in maximum kinetic energies being one to two orders of magnitude greater than the thermal energies.

However, the laser beam–plasma interaction will dictate the film quality and deposition rate. Correlations between film quality and plume diagnostics are frequently made. In spite of complex physics involved in the LAPVD, the process is unique in many aspects such as:

1. complex multi-element materials can be deposited well within the stoichiometric composition of the target;
2. the chamber pressure, target–substrate distance, and target orientation with respect to the laser beam can be easily maintained;
3. the efficiency of the target used is superior to any other technique because a predominant amount of the evaporated material is forward directed and can be collected with high efficiency;
4. the fabrication of multi-layer thin films is fairly straightforward, with rapid substitution of targets into the path of the laser beam;
5. the forward directed evaporant in this process lends itself to novel substrate handling schemes.

The first successful application of the LAPVD process was the deposition of high-quality superconducting thin films from multi-element targets. This process has recently resulted in five more new areas of thin-film fabrication such as ferro-electric, bioceramics, ferrites, magnetic and tribological materials. The success of the LAPVD technique is due to simple processes with stoichiometric thin-film deposition at different atmospheric pressures.

4.3. Laser-assisted chemical vapour deposition

The laser-assisted chemical vapour deposition (LACVD) process is similar to the LAPVD process. Instead of a solid target, a mixture of specific gas media is used to create a plasma by the laser. The laser beam serves as an energy source for decomposing the mixture of gas molecules and is also used to raise the substrate surface temperature. Various materials, metals, semiconductors and insulators in elemental or compound form have been deposited in this fashion, for example, polysilicon and hydrogenated amorphous silicon on quartz, using laser-induced breakdown of an appropriate gas such as silane [5,6]. The vapour of nickel carbonyls can be dissociated to form nickel layers. Also refractory metals such as tungsten, molybdenum and chromium can be deposited from the respective carbonyls. Insulating layers such as TiO_2, TiC can be deposited by dissociating appropriate respective gaseous compounds.

The breakdown of the bonding between the gas molecules will occur by either pyrolysis of photolysis as shown in Fig. 6. In pyrolysis, the substrate is heated by a focused laser beam to a desired temperature by controlling the laser power and irradiation time with the laser beam while the gases decompose by collision excitation with the hot surface (Fig. 6a). The laser-driven reactions are different from those initiated by other CVD sources for the same heat input because of the higher temperatures obtainable in a smaller volume (or region) defined by the focused laser beam. As a result, novel reaction products can be expected. In laser photolysis, photons break the chemical bonds of the gaseous molecules and allow deposition of the products on the substrate (Fig. 6b). An important requirement in photolysis is the need to match the wavelength of the laser beam with the band gap of the reactants. LCVD by photolysis is generally slower than the pyrolysis. For the pyrolysis process, the laser beam should be parallel to the substrate as opposed to normal to the substrate [7]. Fig. 7 shows a schematic diagram for this LACVD technique. The laser is focused through a transparent window. As the deposition reaction is thermally driven, LCVD is exactly analogous and superficially similar to conventional CVD but actually differs in the following ways.

(a) Localized deposition: the most obvious difference is that the deposition is localized because the heat source is localized. Localized deposition is impossible to achieve using conventional CVD.

(b) High deposition rate: LCVD deposition is fast. Coatings of the order of 1 μm thick can be deposited in

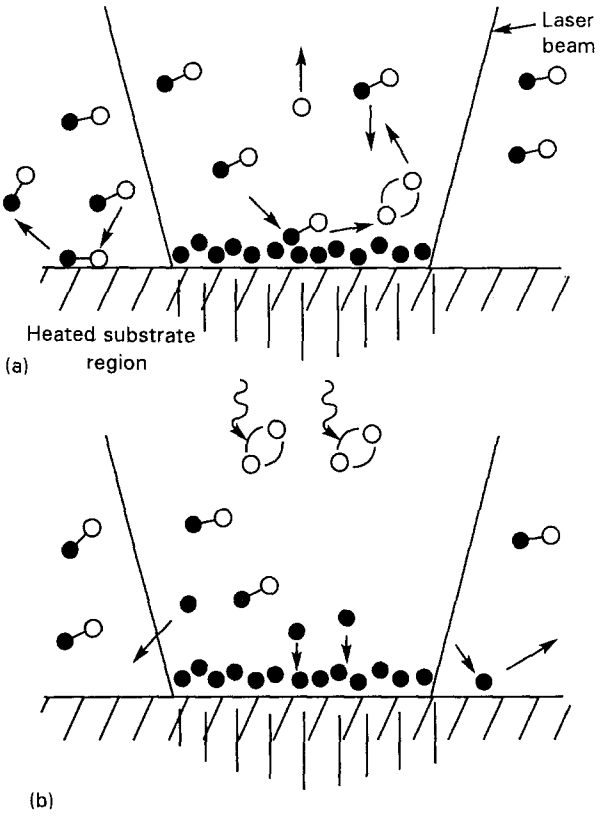

Figure 6 Schematic representation of laser-assisted chemical vapour deposition by (a) pyrolytic and (b) photolytic mechanism.

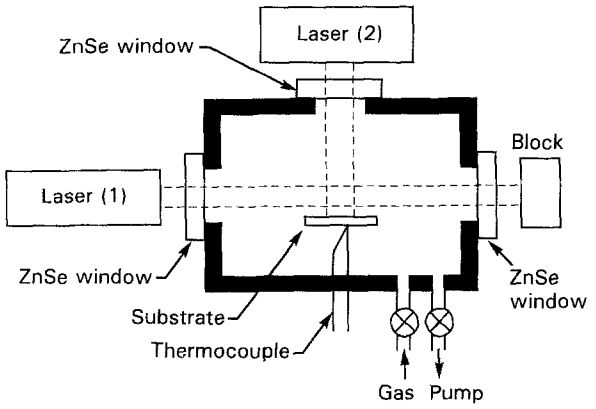

Figure 7 Dual-beam method of laser-assisted chemical vapour deposition.

approximately 0.1 s. For the reactions investigated to date, this rate is two to four orders of magnitude larger than standard CVD rates.

(c) Heating and cooling rate: there is wide range of heating and cooling rates available using LCVD. A very rapid heating and cooling cycle is achievable in LCVD, which make it possible to control the grain size of the deposited film by varying the irradiation waveform. For example, very fine-grained (possibly amorphous) material can be deposited using short laser pulses. In contrast, large-grained material is produced in equilibrium CVD because of the long dwell time at high temperatures.

(d) Gas flow rates: in conventional CVD, deposition rates and film properties are a strong function of gas flow rates and therefore the overall geometry of the substrate and deposition chamber. Because of the localized heating and the fast deposition rates, LCVD should be essentially independent of flow characteristics.

The important independent process variables are (i) incident laser beam power, (ii) beam diameter, (iii) wavelength of the laser beam, (iv) traverse speed or dwell time, (v) surface reflectivity, (vi) chamber temperature, and (vii) substrate thermal properties. The corresponding dependent variables are (i) deposition rate, (ii) composition and microstructure, and (iii) deposit geometry, i.e. thickness and diameter.

4.4. Laser-assisted liquid–solid interaction

This is one of the most recent and novel techniques used to synthesize the product in the form of thin-film or nanosized particles from the liquid phase. Laser irradiation of a solid substrate is carried out while the substrate is immersed in an appropriate liquid having sufficient transparency to the laser wavelength. Subsequent to absorption of laser energy, the surface layer of the solid is rapidly heated and quenched into the liquid medium. This creates a non-equilibrium condition for the liquid near the liquid–solid interface. The liquid molecules break down due to a non-equilibrium condition, thus resulting in a metastable phase. There are three parameters which play an important role in the synthesis of material, namely : wavelength, energy and pulse duration of the laser beam. This technique has not yet been fully explored.

It has been possible to produce layers of carbide, oxide, nitrides of materials such as iron, titanium, tantalum, tungsten and silicon etc., when these materials are laser processed in liquids such as benzene (C_6H_6), water (H_2O), ammonia (NH_3), etc.[8]. The significance of this process is that the solid surface can be processed under appropriate choice of liquid media and the film produced will be free from contamination. For example, diamond thin film was synthesized on the copper substrate from the benzene (C_6H_6) by this technique [9,10] which is discussed in the next section.

5. Laser surface melting

There are many applications of laser and intensive work has been done in areas such as drilling [11], cutting [12]. welding [13–15], surface hardening [16–18], shocking [14], laser surface alloying [19], and cladding [20]. Selective applications of laser-beam processing of advanced materials will be discussed in this review including glazing, surface alloying and cladding, and metal matrix composite coatings formation.

Laser processing provides a number of distinct advantages in meeting the surfacing objectives of wear, corrosion, and oxidation protection and in the refurbishment or build-up of near net-shaped structures. It is possible to produce fine-grained microstructures, amorphous and metastable phases, low porosity, relatively smooth surfaces, small heat-affected zones in the substrate, and good bonding between coatings and substrate. The main disadvantage is high equipment cost. However, the high cost can generally be offset by the unique surface capabilities and the flexibility to use the same laser power source for other materials processing activities including welding, localized surface heating, cutting, and drilling. Through manipulation of processing conditions such as power density, pulse or continuous wave (CW), beam diameter, and traverse speed (Fig. 8), a single laser can

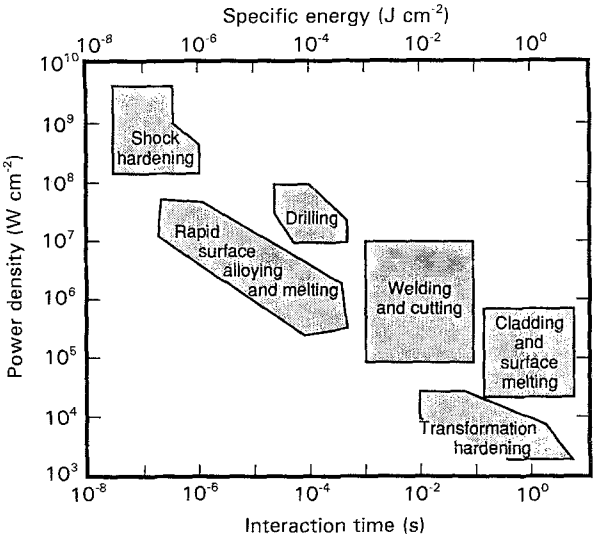

Figure 8 A schematic diagram showing different regimes of laser application as a function of laser power density versus interaction time.

perform several functions. This is one of the reasons why the laser is a popular candidate for flexible manufacturing systems.

5.1. Process variables

Applications and efficiency of laser surface treatments depend on *independent* process variables. The key independent process variables are the wavelength of the laser beam, laser power, pulse or CW laser, size and shape of the laser beam, traverse speed of the substrate with respect to the laser beam, reflectivity/absorptivity of the laser beam, and powder feed rate (for laser surface alloying and cladding). *Dependent* process variables, which are controlled by the above process conditions, are interaction time and cooling rate. Additional cooling can be achieved by applying a copper chill block to the substrate. Thus, a scheme is needed to develop optimized properties of the materials.

5.2. Laser glazing

The laser glazing process is used to modify the surface properties of materials. A thin surface layer is rapidly melted and solidified to produce a microstructure different from that of the bulk material. High cooling rates of the molten surface layer can promote the formation of amorphous material, metastable phases, and fine-grained microstructures, resulting in improved surface properties such as wear, corrosion, and fatigue resistance. The principal advantage of laser glazing is that it alters the microstructure without changing the composition, as compared to laser surface alloying and cladding which are intended to alter the composition of the surface.

In the laser glazing process, laser energy is absorbed by the surface of the solid, melts the surface, and the melt front propagates into the bulk to a depth determined by deposited energy and materials properties. The melt velocity is controlled by the rate of energy deposition, the absorbed depth in the solid and liquid phases, and the thermal properties of the solid. After the surface has been melted, the molten layer resolidifies as heat flows into the underlying substrate. Resolidification occurs at the liquid–solid interface and the interface moves to the sample surface with a resolidification velocity, v. Because of high-temperature gradients, v can be very large. Temperature gradients ($\partial T/\partial Z$) of up to 10^{19} K cm^{-1} and corresponding quenching rates of up to 10^{11} K s^{-1} can be readily achieved. Increase in $\partial T/\partial Z$, results increased v up to 20 m s^{-1}. As far as microstructure in laser-glazed materials is concerned, one can expect either amorphous, microcrystalline, or epitaxial growth structures, depending upon the chemistry of the material and the melting and solidification rates.

5.3. Laser surface alloying (LSA)

Laser surface alloying is shown in Fig. 9 [20]. Consider a preplaced powder or thin film on the substrate (Fig. 9a) which is then exposed to a laser beam. Depending upon the top surface characteristics of the precoated film, a certain amount of energy would be absorbed and instantaneously transferred to the film and substrate. The top surface region rapidly reaches its melting point and transfers the majority of its heat energy to the substrate. A liquid/substrate interface is established and moves towards the substrate, which is the major sink for heat energy (Fig. 9b, c). Within a fraction of a second, (< 1 ps), the coated film completely melts and forms a molten region inside the substrate (Fig. 9d). The depth of melt region depends upon the laser power and interaction time. At this stage, there would be interdiffusion, or mixing, of the precoated thin film with the substrate melt region by a convective fluid flow mechanism. For a fraction of a second, the liquid/solid interface is stationary (Fig. 9d), and then resolidification occurs rapidly. During rapid solidification, the solid/liquid interface moves upwards as shown in Fig. 9e. Interdiffusion in the liquid melt region continues until it is completely solidified. As the rate of solidification is very high, interdiffusion in the solid state is negligible. The alloy of A and B is thus produced in the substrate (Fig. 9f). The cross-section of the substrate would clearly reveal the formation of the new alloy (having a composition A_xB_{1-x}) within the substrate.

The modified surface thus produced can have superior chemical, physical or mechanical properties. The depth of the alloy zone can be controlled by the power and the dwell time of the laser beam. Depending upon the type of alloy required at the surface, a less-expensive base material can be locally modified to improve resistance to corrosion, erosion, wear, and oxidation.

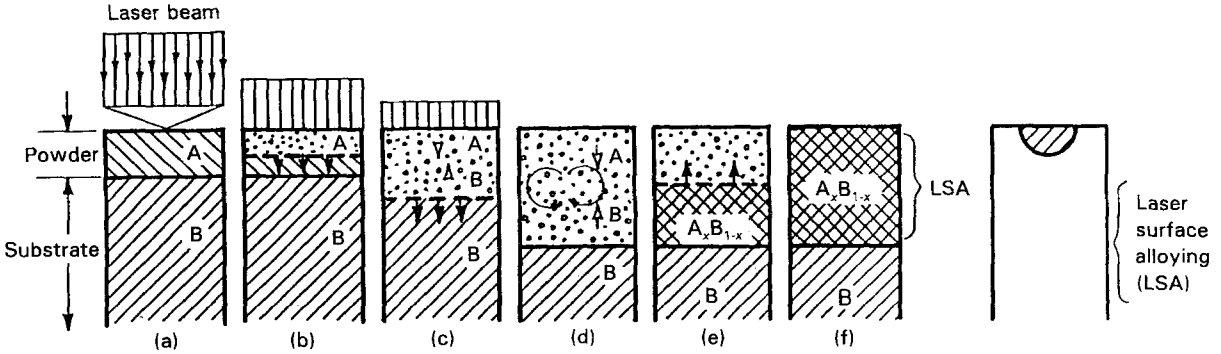

Figure 9 A schematic diagram showing the different steps involved during the laser surface alloying process [20].

5.4. Laser surface cladding (LSC)

Laser surface cladding is a process similar to laser surface alloying except that dilution by the substrate material is kept to a minimum (Fig. 10a–g). In addition, a clad layer is formed on the substrate surface. Similar to LSA, this process also provides tailored surface properties. By this process, the corrosion, wear and oxidation resistance can be improved.

Laser cladding has many advantages over alternative methods, such as plasma spray and arc welding. These advantages include a reduction in dilution, a reduction in waste due to thermal distortion (very little energy is absorbed by the substrate in comparison with plasma spraying and arc welding), a reduction in porosity, and a reduction in post-cladding machining costs. Because the material can be accurately placed, a rapidly solidified microstructure is possible and a relatively smooth surface is produced. Laser cladding offers the potential for generating new materials with metastable phases (e.g. extended solid solution due to the inherent rapid solidification associated with the process).

In laser cladding and alloying processes, alloyed powder is transported by an inert gas stream and injected through a nozzle directly into the centre of the laser beam/molten pool and on to the moving substrate. The powder can be delivered into the melt-pool region by two methods: injecting the powder at an angle into the melt-pool region (Fig. 11) or injecting into the melt-pool region co-axially along with the laser beam. Instead of powder, prealloyed wire can also be used, A uniform clad layer is produced by the above methods.

6. Microstructural evolution of laser-processed materials

6.1. Photon-assisted processing of materials

As mentioned above, the photon-assisted processing of materials has recently gained importance in the processing of thin films for electronic industries. This process has not yet been fully exploited. The biggest challenge in the electronic industries is to fabricate good-quality microchips at low temperatures. The main requirements for fabricating high-quality microchips are:

(i) low-temperature growth of thin films;
(ii) epitaxial growth of thin films;
(iii) high-quality defect-free thin films;
(iv) stoichiometric composition of thin films;
(v) preferred growth equiaxed versus columnar growth.

6.1.1. Laser-assisted synthesis of diamond from liquid hydrocarbon

Single-crystal (1 0 0) and polycrystalline copper specimens [9, 10] were immersed in benzene (C_6H_6) liquid (Fig. 12) and irradiated with high-power laser pulses from an Excimer laser ($\lambda = 308$ nm, $t = 30 \times 10^{-9}$ s, $E = 1$–$4\ J\,cm^{-2}$). The benzene liquid layer above the specimens was about 3 mm and the copper specimens were usually 10 mm × 10 mm. Thin films grown on the copper substrate, as a result of pulsed laser irradiation ($E = 3\ J\,cm^{-2}$ and 5 pulses), was examined by high-resolution transmission electron microscopy as shown in Fig. 13. The corresponding selected-area electron diffraction pattern (inset) shows the ring patterns representative of a fcc polycrystalline material. The characteristics of (1 1 1) and (2 2 0) rings were indicative of the presence of diamond cubic tetrahedron in the film [9, 10].

The diamond produced by a laser–liquid–solid interaction process was confirmed by using it as a seed for subsequent diamond growth by a hot filament CVD process. Fig. 14a–f show scanning electron micrographs of a high density of diamond crystallites in the laser-irradiated area as a function of laser pulses (i.e. at a laser energy of $3.7\ J\,cm^{-2}$ and 1, 2 and 4 pulses). In certain areas, the density of diamond was significantly higher and appeared as a continuous diamond film. It was interesting to note that, as the number of laser pulses increased from 1 to 4, the density of diamond crystallites also increased. At 4 pulses, an almost continuous film was achieved (Fig. 14e and f). The extent of the continuous film was about 40–50 μm. Diamond crystallites appeared to be faceted in nature with an average size of about 2–3 μm. The above SEM results indicate that the laser interaction produced fine diamond particles which acted as seeds for further growth of diamond.

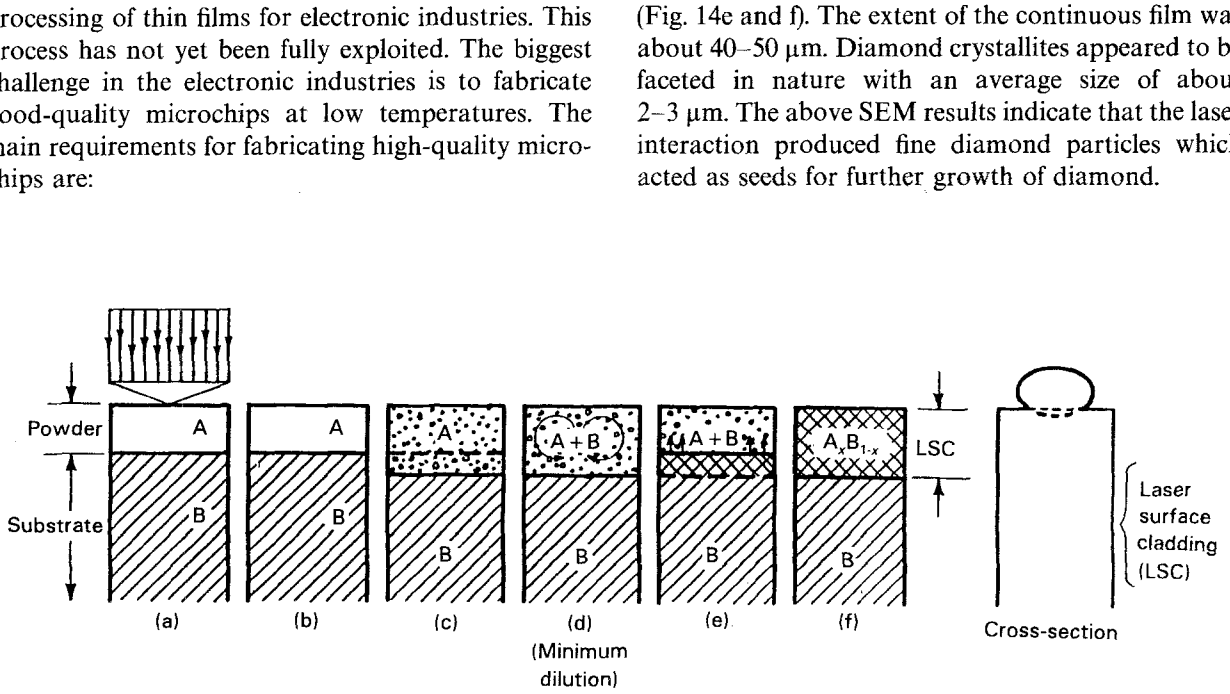

Figure 10 A schematic diagram showing the different steps involved during the laser surface cladding process.

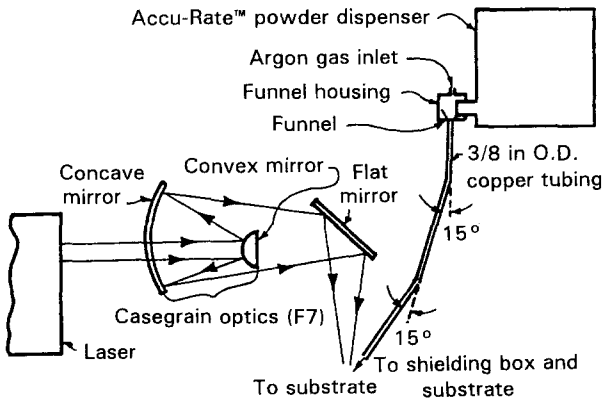

Figure 11 A schematic diagram showing the side delivery of powder alloy into the melt pool region.

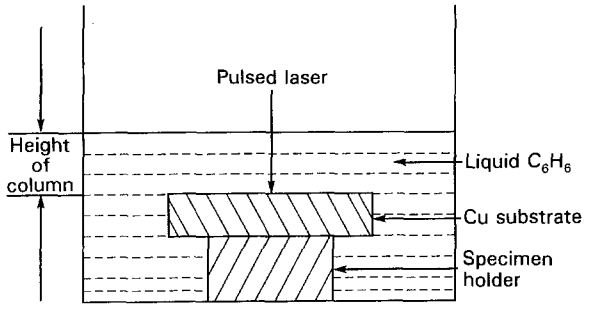

Figure 12 Schematic diagram showing laser–solid interaction in the liquid hydrocarbon (benzene, C_6H_6) medium.

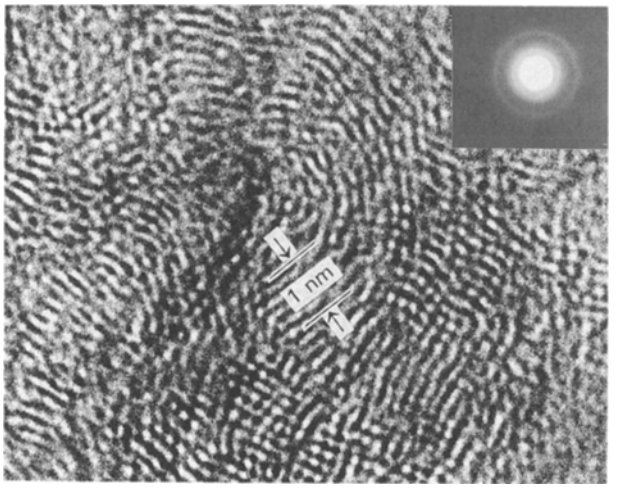

Figure 13 High-resolution transmission electron micrograph showing nanocrystalline diamond thin film with carbon atoms having cubic pattern. The corresponding diffraction pattern is shown as an inset [10].

6.1.2. Epitaxial growth of TiN films on (100) silicon substrate by LAPVD

Titanium nitride (TiN) coatings and thin films have found applications ranging from corrosion and erosion-resistant coatings to diffusion barriers in advanced integrated circuit devices to wavelength-selective films. TiN films deposited by various techniques including CVD, ion plating, and magnetron sputtering, have produced a polycrystalline microstructure. These polycrystalline films tend to grow in a columnar way with grain boundaries normal to the substrate. In the columnar structure, faster diffusion along the grain boundaries makes these films susceptible to environmental degradation and reduces their effectiveness as a diffusion barrier. The above problems in polycrystalline films can be solved by producing an equiaxed microstructure. Polycrystalline TiN films with equiaxed-grain microstructure were produced by the CVD process above 900 °C but at such a high temperature, TiN thin-film growth (> 900 °C) is unacceptable to the electronic industries. Recently, polycrystalline TiN films with equiaxed-grain microstructures were produced by LAPVD in the temperature range 400–500 °C on a silicon substrate [10]. The details of epitaxial growth and properties of these films are discussed below.

Laser-assisted physical vapour deposition (LAVPD) of TiN was carried out using a pulse KrF eximer laser (wavelength 248 nm, pulse duration 25 $\times 10^{-9}$ s, repetition rate 5 Hz). The laser beam was focused on the target (TiN) to obtain an energy of $\sim 10\,J\,cm^{-2}$ at a 45° angle of incidence. The target was held parallel to a cleaned (100) silicon substrate (Fig. 4). The deposition chamber was evacuated to a base pressure of about 1×10^{-7} torr using a turbomolecular pump and depositions were carried out in the temperature range 600–700 °C. Some samples were deposited with TiN at 350 °C followed by high-temperature deposition. The deposition rate was typically $0.1\,nm\,s^{-1}$. A 20 min deposition at 5 Hz resulted in an approximately 100 nm thick TiN film.

Fig. 15 shows X-ray diffraction traces of TiN films on a (100) Si substrate. The pattern contains (200) and (400) TiN reflections together with (400) Si diffraction spots, indicating that the TiN film is textured with [100] of TiN aligned with [100] of silicon. The lattice constant of TiN from these traces was determined to be 0.4222 nm. In order to study the inplane alignment of the TiN film with respect to the silicon substrate and its epitaxial nature, cross-section specimens were prepared and examined using a high-resolution Akashi 002B transmission electron microscope. Fig. 16a is a high-resolution transmission electron micrograph (HRTEM) containing the TiN/Si interface with ⟨110⟩ normal to the specimen. The {111} planes in silicon with 0.314 nm spacing are aligned with {111} TiN planes with 0.244 nm spacing. The dislocations associated with extra half planes terminating at the interface are clearly observed at the interface. These dislocations relieve some of the lattice misfit strain between the TiN layer and the silicon substrate. Fig. 16b shows a high-resolution transmission electron micrograph from another area where both sets of {111} planes in the silicon and TiN are clearly visible. The micrograph clearly shows epitaxial growth even in the presence of an interfacial oxide layer (~ 0.7 nm thick). This may occur as a result of lateral epitaxy originating from pinholes and growing over the surrounding thin oxide layer. Although the film is epitaxial, it contains a high density of dislocations. Fig. 17a–c show selected-area diffraction (SAD) patterns of silicon (a), TiN (b), and the interface

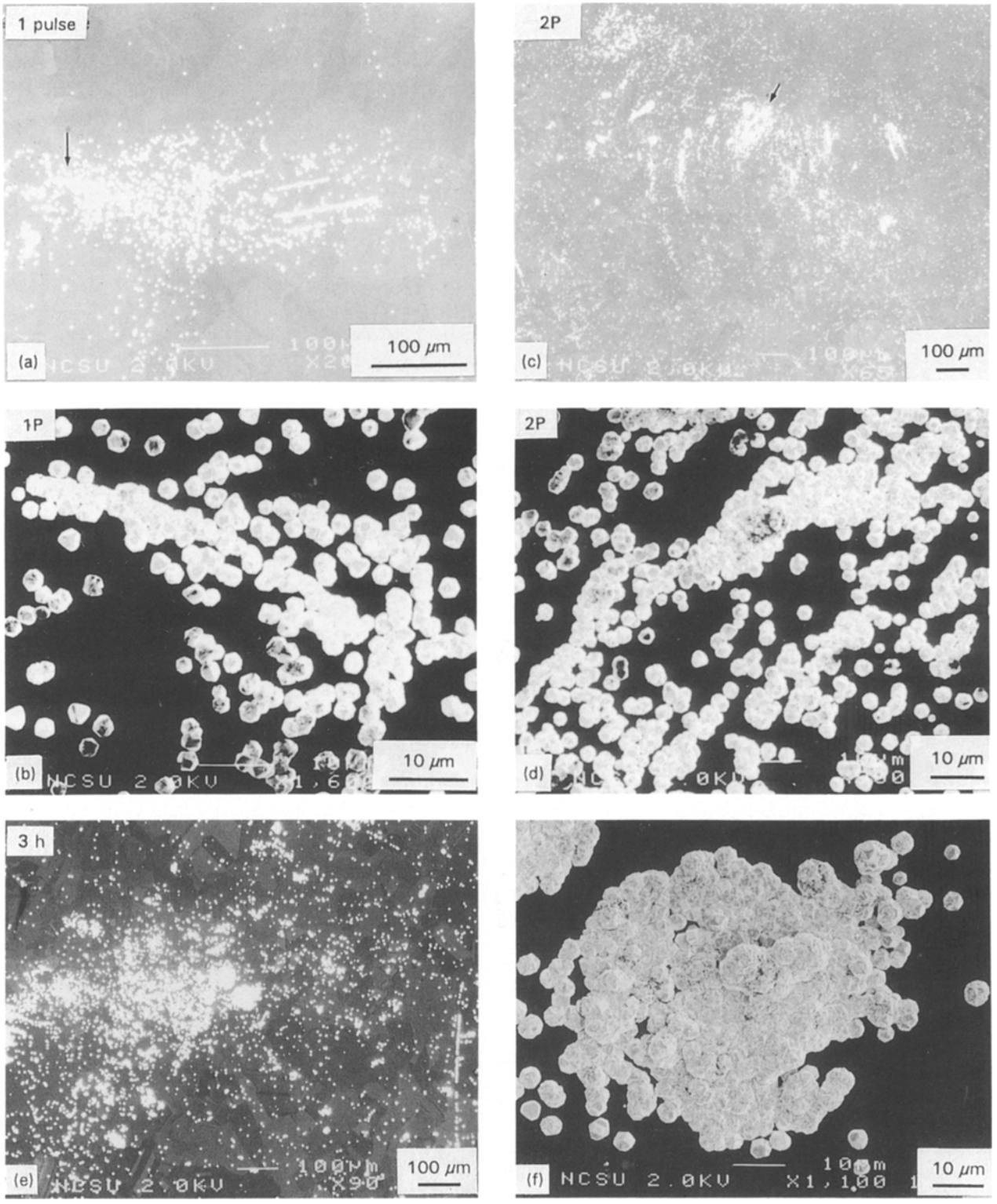

Figure 14 Scanning electron micrographs showing selective and relatively high density of diamond growth on the laser-irradiated region of the sample. Copper samples were irradiated with laser energy of 3.7 J cm^{-2} at pulses 1, 2, and 4, respectively. Subsequent diamond was grown by the HFCVD process at 800 °C for 3 h [10]. (a, b) number of laser pulses 1; (c, d) number of laser pulses 2; (e, f) number of laser pulses 4.

of TiN and silicon (c) from (1 1 0) cross-section specimens. The TiN and silicon diffraction spots that aligned with each other were the fourth-order diffraction spot of TiN with the third-order spot of the silicon substrate. The alignment was within 4%. These patterns clearly establish cube-on-cube alignment between the TiN layer and the silicon substrate. Fig. 18 shows Rutherford back scattered (RBS) spectra (random and aligned) from the above specimens. The X_{min} value (ratio of random to aligned channeling yield) was found to be 10%–20%, indicating epitaxial films with a high defect density consistent with HRTEM observations. In conclusion, the epitaxial TiN films can be grown on (1 0 0) silicon substrate with cube on cube ⟨1 0 0⟩ alignments. Under these conditions, three units of silicon are found to match with four units of TiN with about 4% mismatch [10].

By the LAPVD technique, multiple layers of superconducting $YBa_2Cu_3O_{7-\delta}$ (epitaxial) and ferroelectric $Pb_{0.52}Zr_{0.48}TiO_3$ epitaxial and textured thin films

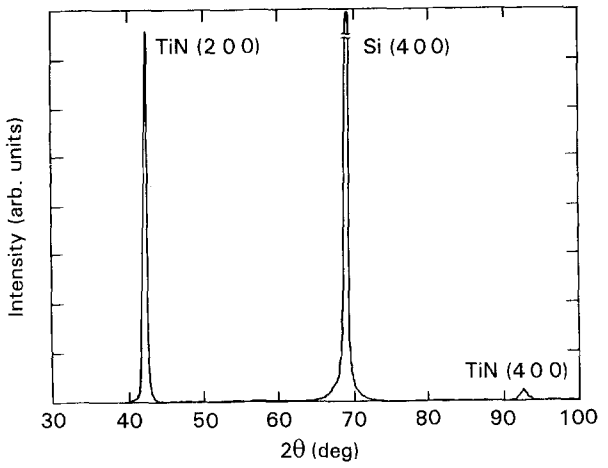

Figure 15 X-ray diffraction intensity versus incident angle plot showing (1 0 0) peaks from a TiN film and (0 0 1) silicon substrate.

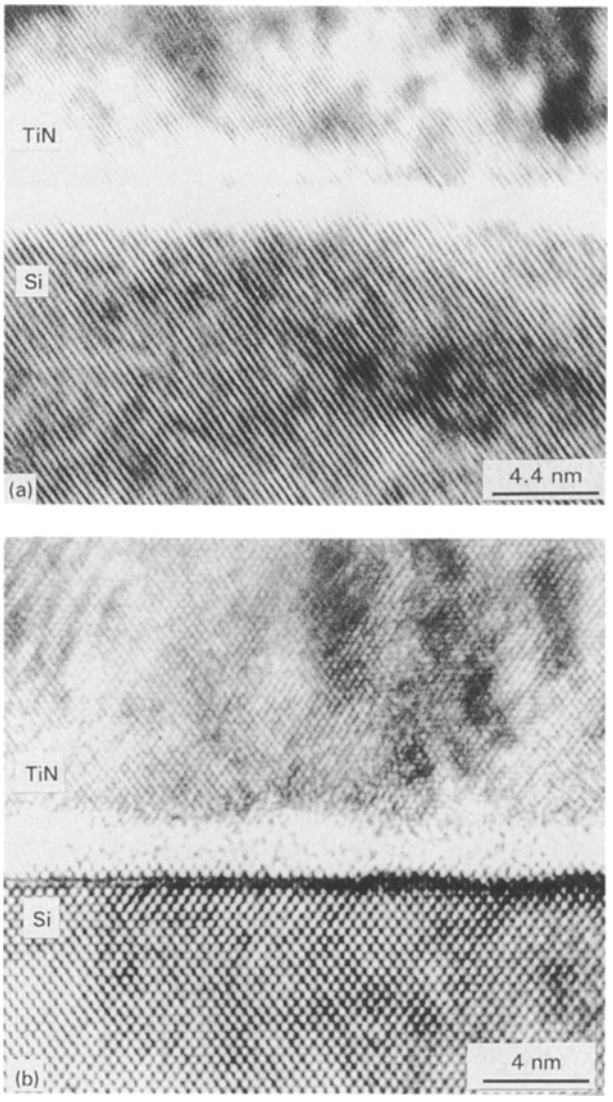

Figure 16 High-resolution transmission electron micrographs from ⟨1 1 0⟩ cross-section showing {1 1 1} planes from silicon substrate and TiN film. (a) The termination of planes associated with dislocations near the interface is clearly observed. (b) Higher resolution reveals both sets of {1 1 1} planes lying parallel to the electron beam.

have been successfully grown on the TiN/Si substrate where TiN served as a buffer layer [1]. These multilayer structures are expected to play a prominent role in high-temperature superconductor and ferroelectric integrated circuit technology.

6.2. Laser surface melting (glazing)

Laser glazing can be done with either a pulsed or a continuous wave (CW) laser. A pulsed laser is often used to achieve very rapid heating (melting) and cooling (solidification) of the near surface of materials with quenching rates of 10^6–10^{14} K s^{-1} [21]. Pulsed lasers have been extensively used in the micro-electronics industry for the glazing of semiconductors [22, 23]. This technique is also used to seal the surface of plasma-sprayed thermal barrier coatings (TBC) on a nickel substrate to improve its high-temperature corrosion resistance [21, 24]. The plasma-coating process is used to apply a variety of coatings on parts and also to fabricate near net-shaped parts with properties equivalent to the wrought alloy. However, the plasma spray coatings contain defects such as porosity, non-bonded interface, and unmelted powder particles which reduce the mechanical properties of the materials. The microstructure and mechanical properties of plasma-coated materials can be improved by the laser-glazing process. This has been demonstrated by laser glazing on the vacuum plasma-coated NARloy-Z (Cu–3 wt%Ag–0.5wt%Zr). The microstructure of the laser-glazed area was free from the above-mentioned defects (Fig. 19).

The NASA–Marshall Space Flight Center is directing an effort to enhance the life of many component parts or to refurbish parts of the space shuttle main engine (SSME) after each mission [25]. Laser glazing has shown attractive applications to enhance the life of many components such as the liner of the main combustion chamber (MCC) of SSME. The most critical part of the MCC is its liner (called hot wall) which is made of wrought NARloy-Z (Cu–3% Ag–0.5%Zr). The silver is added to the NARloy-Z for precipitation strengthening in the form of a fine dispersion of silver into the copper matrix [26]. The zirconium is added to absorb oxygen traces present in the copper matrix by forming Zr_2O_3. The life of the liner depends upon its microstructure, which degrades with hot-firing cycles due to high-temperature exposure. The liner develops micro-cracks due to grain-boundary sliding, overageing, and grain boundary precipitation. Laser glazing has been shown to improve the microstructure of the wrought alloy.

Fig. 20 shows the microstructural evolution in the wrought NARloy-Z after exposure at high temperatures ranging from 580–760 °C for up to 96 h. Undesirable grain-boundary precipitates and precipitate-free zones (PFZ) were observed which decreased the life of the MCC liner. Once these precipitates are formed, they are difficult to put back into solution by heat treatments, with the exception of remelting. Laser glazing was found to be very useful to refine the microstructure of wrought NARloy-Z (Fig. 20). Fine-grained microstructure with uniform distribution of

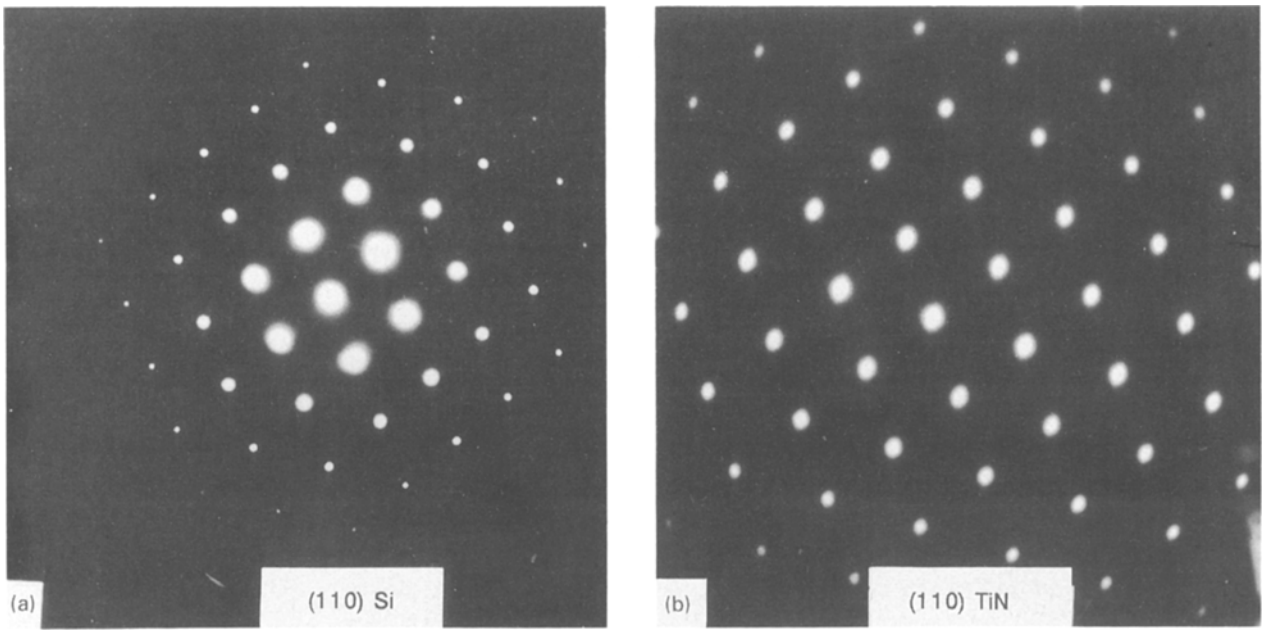

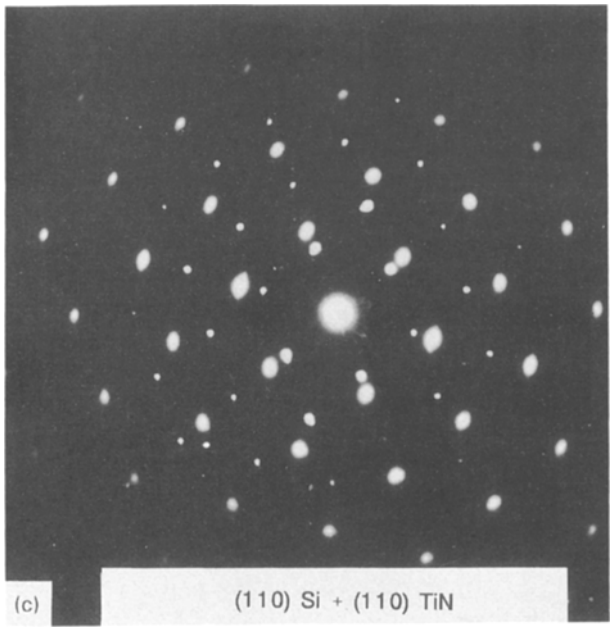

Figure 17 Selected-area diffraction patterns from the cross section of Fig. 16, under same camera length at different locations; (a) Si (1 1 0), (b) TiN (1 1 0), and (c) interface containing both Si (1 1 0) and TiN (1 1 0).

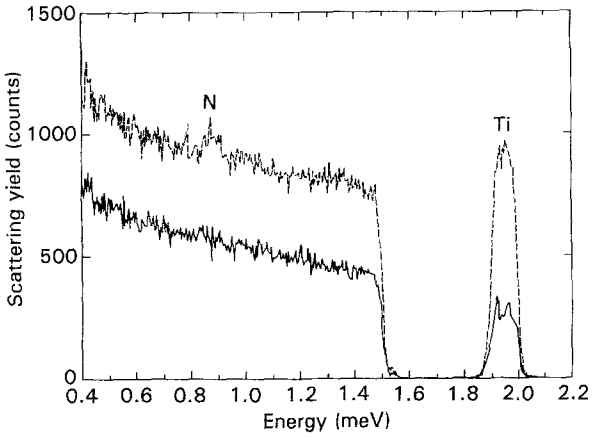

Figure 18 RBS spectra of a TiN film on Si (1 0 0) substrate in (———) aligned and (– – –) random directions. The minimum yields suggest that epitaxy is superior near the surface compared to that at the interface.

second phases and extended solid solubility of solute atoms (zirconium in the present case) in the copper matrix of laser-glazed NARloy-Z was obtained by laser glazing which resulted in an improvement in the thermal stability and age hardening of the alloy Fig. 21 and 22). Thus, the laser-glazed MCC liner will have more life than the current liner [26, 27]. As a matter of fact, laser glazing can also be used for refurbishing the MCC liner after thermal exposure from a series of hot firings. This concept can also be applied to other components for rejuvenation of their life.

6.3. Cladding

6.3.1. Oxidation-resistant coating for titanium alloys

Titanium-based alloys are high-strength and light-weight materials used extensively in the aerospace industries for airframe structure and component parts in the aircraft engines (e.g. airfoils). However, titanium alloys have poor oxidation resistance at temperatures above 600 °C. The most critical section of the airfoil is its tip which is generally exposed to high temperatures > 500 °C during engine operating conditions. The laser cladding of niobium on the tip of airfoils (Ti–6 wt% Al–4 wt% V alloy) was found to be very successful for three reasons: the laser beam was able to follow the contour of the airfoils, good bonding between the laser-clad niobium and airfoils was obtained, and thickness and composition of the coating were easily controllable (Fig. 23).

One of laser-clad alloys, (50%Nb–50% Ti) on the Ti–6%Al–4% V substrate was heated in an electric furnace in air to a temperature of 1000 °C for 48 h. The oxide layer which formed on the commercial Ti–6–4 alloys was about 500 μm thick, porous, and tended to

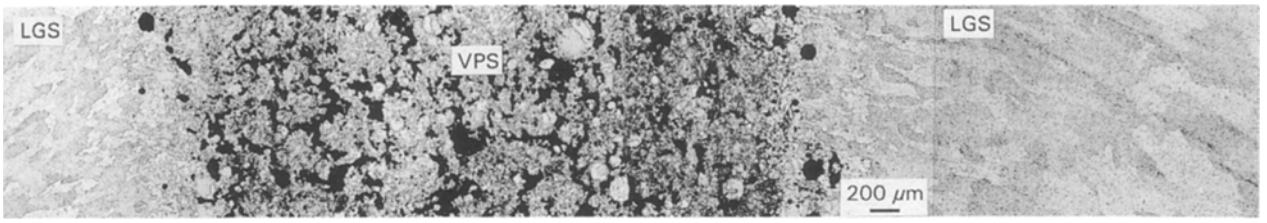

Figure 19 Optical micrograph showing the elimination of defects such as cavities, voids, unmelted particles, etc., present in the vacuum plasma-sprayed (VPS) NARloy-Z by laser glazing. The central section represents VPS and the outer sections represent laser-glazed areas.

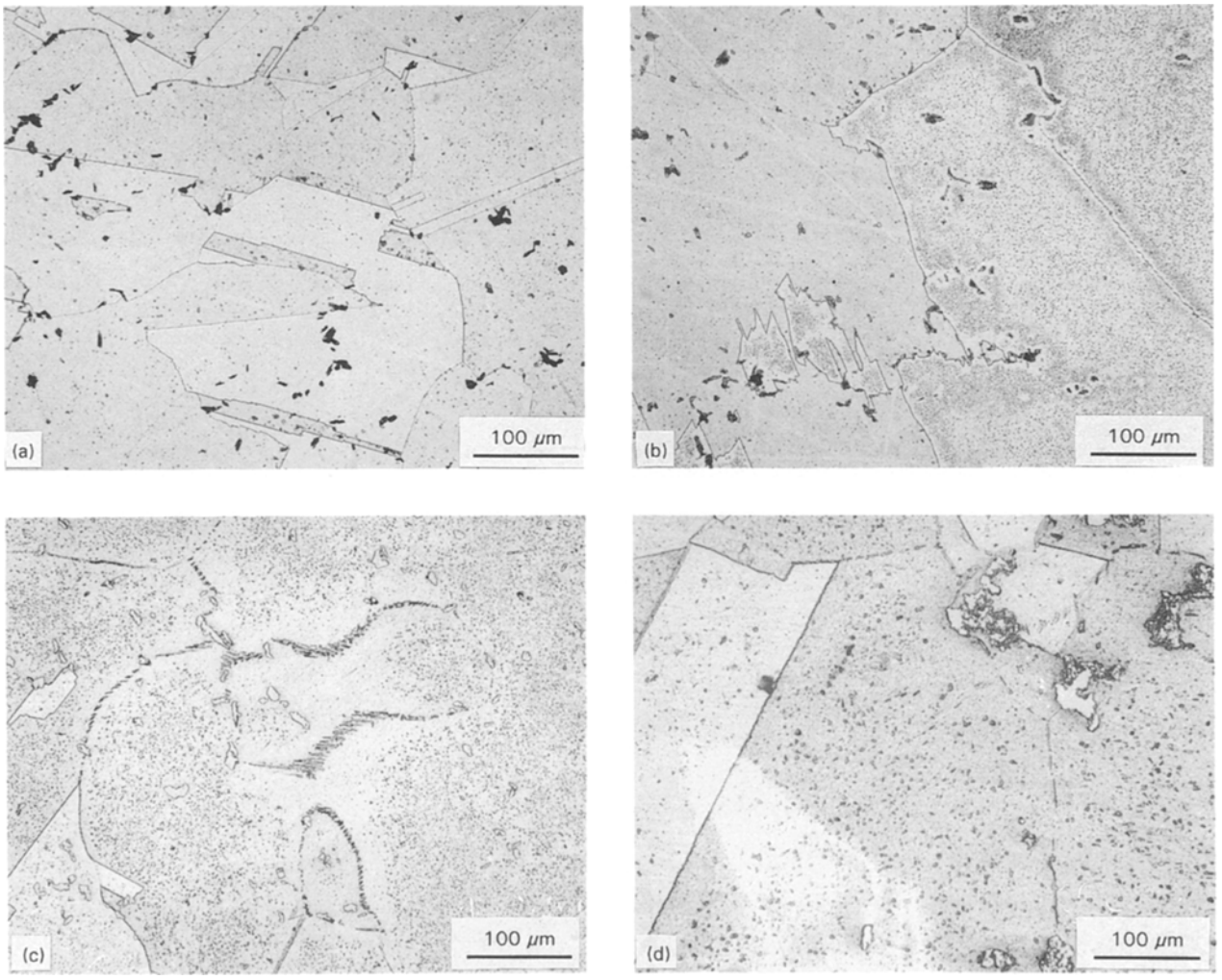

Figure 20 Optical micrographs of the wrought NARloy-Z are showing coarse-grained microstructure with coarse precipitates in the matrix and at boundaries, and precipitate-free zones after exposure at high temperatures for 24 h: (a) wrought alloy, (b) 590 °C, (c) 700 °C and (d) 760 °C.

flake off or spall from the substrate. In contrast, the oxide layer formed on the laser-clad (Nb + Ti) alloy was thin (~ 100 μm) and had a good adherence (Fig. 24). Thus, it was evident that the laser-clad (Nb + Ti) alloy had better oxidation-resistance properties than the Ti–6% Al–4% V alloy.

6.3.2. High-temperature environmentally resistant materials

Nickel-based alloys are commonly used as high-temperature environmentally resistant materials in the aircraft and turbine industries. There are mainly three challenges for the nickel-based alloys: high-temperature stability, oxidation resistance, and high-temperature mechanical properties. Various processing techniques have been used in alloy development such as ion-beam mixing, laser surface alloying, laser surface cladding, and sputtering, but each process has its own limitations. The laser-cladding process gave the most promising results in improving the oxidation resistance of nickel-based superalloys used in turbine engines. It has also shown the most promise for satisfying the above requirements as discussed below.

Recently, considerable attention has been paid to extending the solid solubility limits of rare-earth

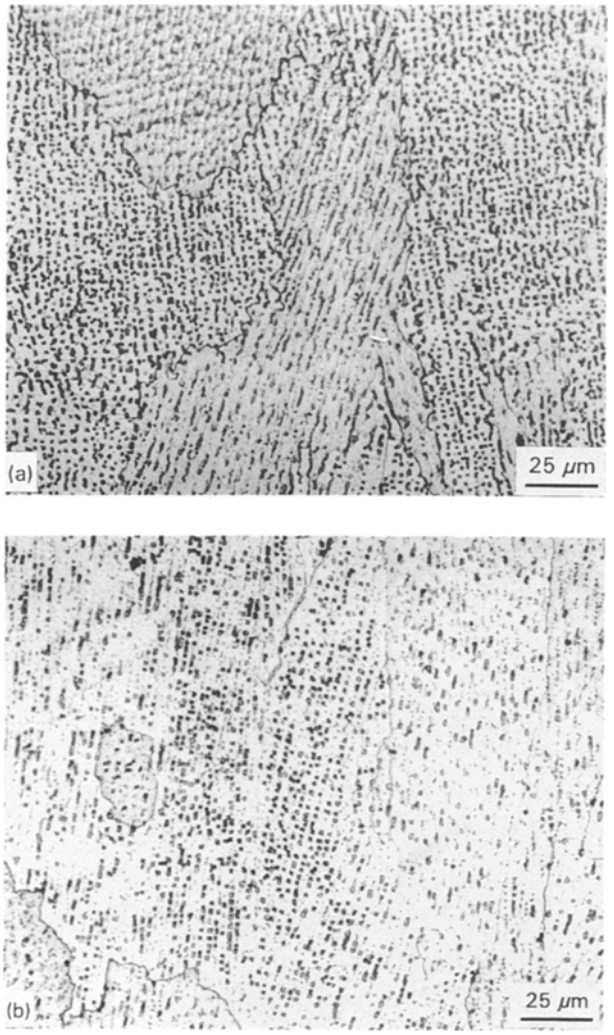

Figure 21 Optical micrographs of the laser-glazed wrought NARloy-Z showing uniform distribution of second phase (silver precipitates) with refined microstructure; (a) as-glazed, (b) after exposure to high temperature (1400 F, 760 °C) for 24 h.

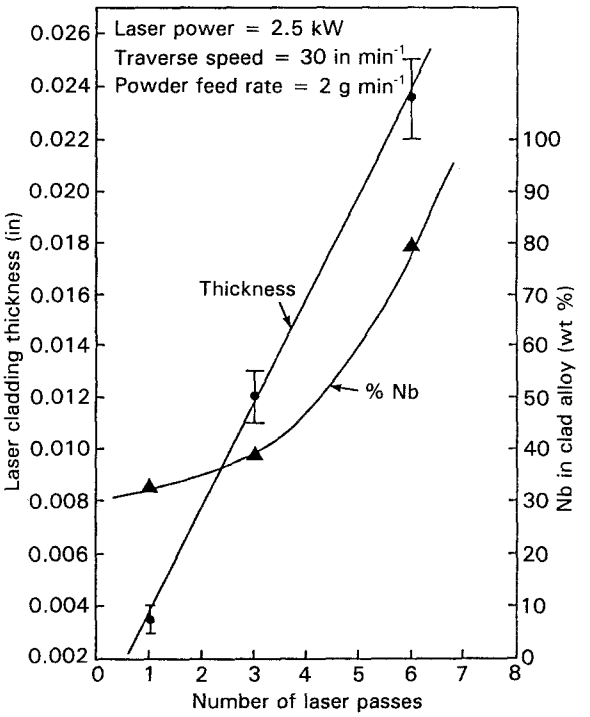

Figure 23 Plot of laser-clad thickness versus number of laser passes during the laser cladding process and corresponding composition of the clad alloy.

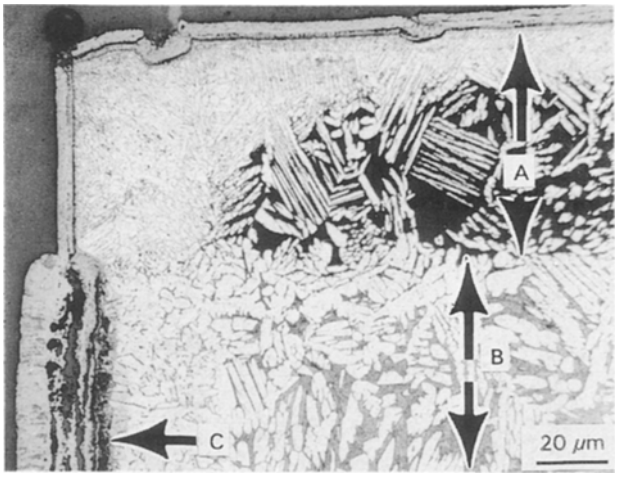

Figure 24 Optical micrograph of laser-clad (Ti + Nb) alloy on the Ti–5%Al–4%V showing the variation in thickness of the oxide layer formed (C) on the laser clad alloy (A) and substrate (B) after exposure to air at 1000 °C for 48 h.

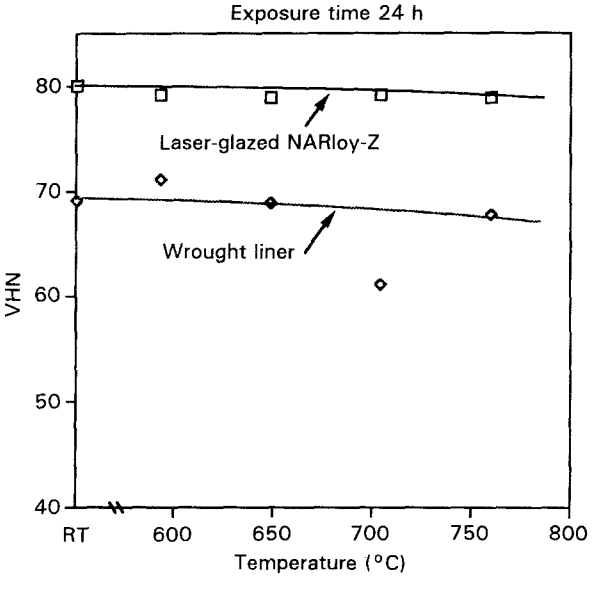

Figure 22 Hardness change in the wrought and laser-glazed NARloy-Z as a function of exposure temperature (590–760 °C).

additions (e. g. yttrium, hafnium and cerium) in nickel-based superalloys to improve their oxidation resistance at elevated temperatures. Under equilibrium conditions, the maximum solid solubility of rare-earth metals (hafnium, rhenium, yttrium, cerium) is < 0.2 wt% at room temperature. Alloys produced by laser surface cladding of Ni–Cr–Al–Hf–Re resulted in a uniform distribution of alloying elements in the clad matrix with extended solid solubility, greatly refined microstructure, and the formation of metastable rhenium- and hafnium-rich phases [28–30]. In the laser-clad Ni–Cr–Al–Hf–Re alloys, the main phases are gamma (nickel-based matrix), gamma prime (Ni_3Al structure), and rhenium- and hafnium-rich precipitates (Fig. 25). The volume fraction and size of

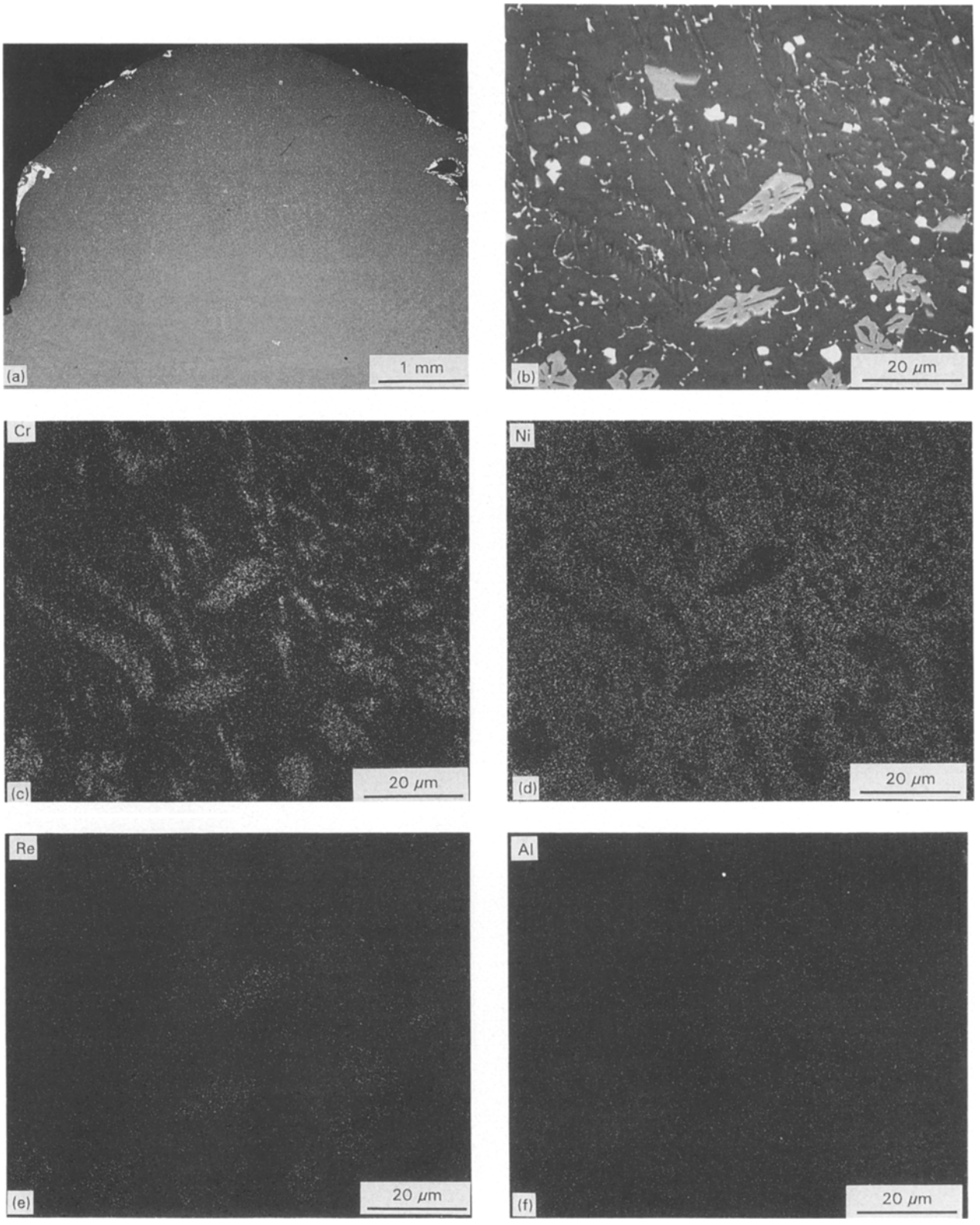

Figure 25 Scanning electron micrographs showing the distribution of each alloying element, undissolved hafnium particles, and non-equilibrium phases present in the laser-clad Ni–Cr–Al–Hf–Re alloy matrix. (a) Clad region showing uniform distribution of undissolved hafnium particles, (b) the formation of second phases in the clad matrix, (c–g) the distribution of alloying elements (chromium, rhenium, aluminium, hafnium) in the laser-clad nickel matrix.

these phases (e.g. gamma prime) depends upon the laser processing conditions (Fig. 26). The size of the gamma prime precipitates increases as a function of hafnium concentration (Fig. 27). The morphology of gamma prime precipitates also depends upon the rate of solidification and its microchemistry (Fig. 28). Owing to rapid solidification that occurred during laser cladding, the solid solubility of hafnium was increased to ~ 30 wt% in gamma prime precipitates (Fig. 29). Thermal stability of the clad alloy depends upon the volume fractions of metastable phases, undissolved hafnium powder particles present, and solid solubility of the alloying additions in the gamma prime precipitates [31–33]. The thermalstability of a laser-clad

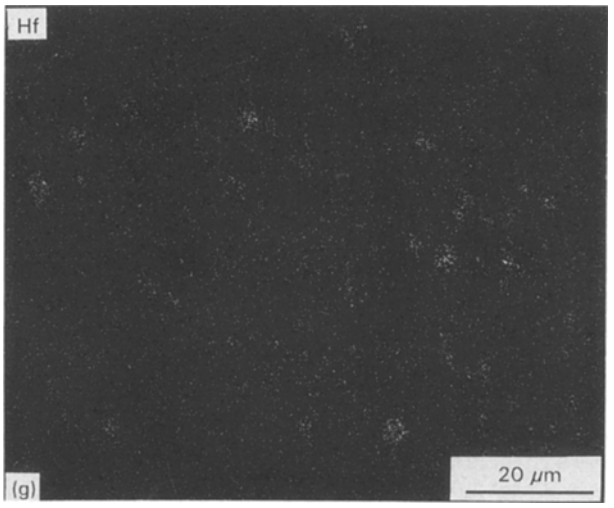

Figure 25 (g)

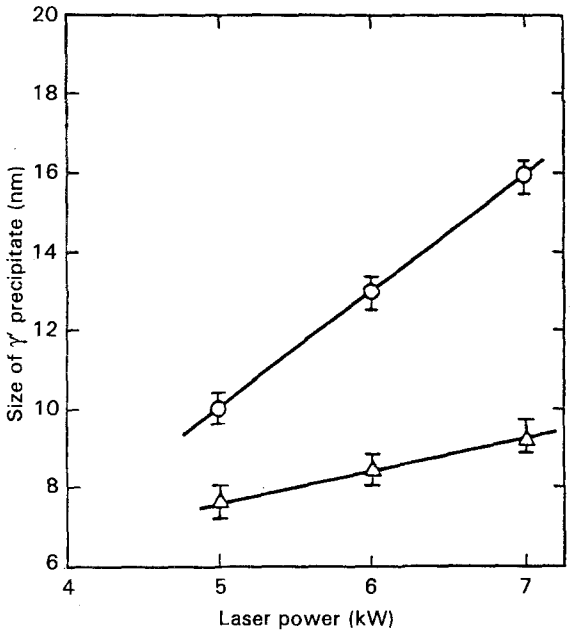

Figure 26 A plot of size variation of fine gamma prime precipitate as a function of laser power at two traverse speeds: (○) 6.35 mm s^{-1}, (△) 14.8 mm s^{-1}.

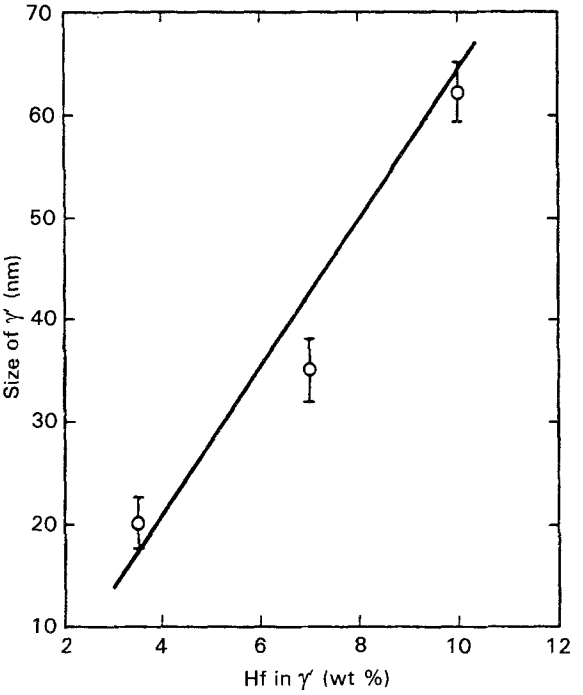

Figure 27 A plot of size variation of fine gamma prime precipitates as a function of hafnium content.

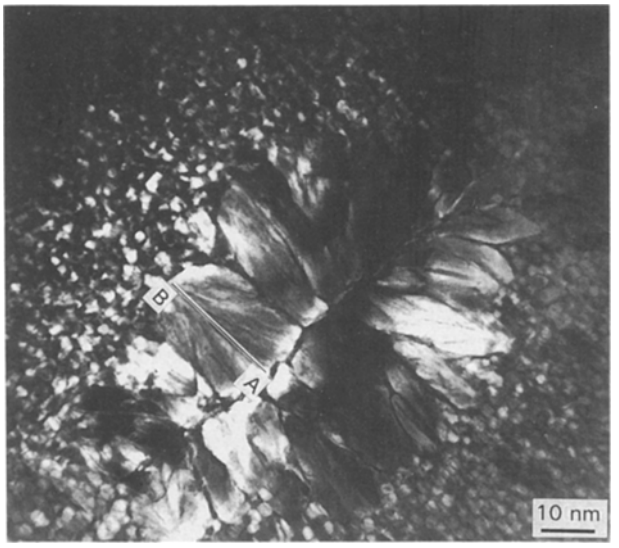

Figure 28 Transmission electron micrograph from the laser-clad region showing the growth of coarse gamma prime precipitates in the middle of grains together with fine gamma prime precipitates.

Ni–Cr–Al–Hf alloy was found to be 1300 °C, which was higher than the nickel-based Rene 95 alloy (1200 °C) as shown in Fig. 30.

Potential applications for laser cladding exist in the auto, turbine and aircraft industries, for example, the critical portion of a turbine airfoil is its tip which is exposed to a relatively higher temperature than the normal operating temperature. The airfoil tip rubs against the liner of the engine casing due to rotation and expansion. Thus, the tip of the turbine airfoil must have high thermal stability, oxidation resistance, and wear resistance.

To meet these challenges, metal matrix composite coatings were developed which have both wear and oxidation resistance. The coating should have uniform dispersion of wear-resistant ceramic powder particles (such as Al_2O_3, HfC, SiC, etc.) into the oxidation-resistant nickel-based matrix. The composite coating was developed by injecting prealloyed powder of Ni–Cr–Al–Hf co-axially together with the laser beam into the melt-pool region. Simultaneously, the wear-resistant ceramic particles were injected at an angle into the melt region, and away from the laser-melt region (as shown in Fig. 31). The ceramic particles did not get a chance to be exposed or interact with the laser beam. Owing to rapid solidification, ceramic particles were entrapped on surface of the substrate, as shown in Fig. 31. The volume fraction and distribution of the ceramic particles entrapped in the matrix were also dependent upon the laser-processing conditions as discussed above. Fig. 32 shows uniform distribution of ceramic Al_2O_3 particles into the nickel

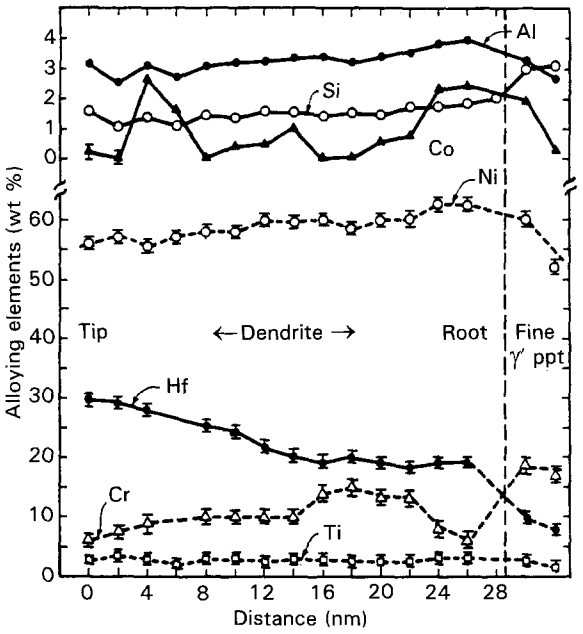

Figure 29 STEM X-ray microanalysis of dendritic growth of gamma prime across their growth direction.

matrix (Ni–Cr–Al–Hf alloy). Additional rapid quenching rates were achieved utilizing a copper chill block which further refined the microstructure of the clad alloy with extended solid solubility and a minimum heat-affected zone. Thus, new engineering materials can be tailored by the laser-cladding process and meet the challenges of turbine industries.

6.3.3. Formation of metastable phases

As mentioned above, the solid solubility of hafnium was extended to ~ 33 wt% in gamma prime precipitates by the laser cladding process. Similarly, there was also an extended solid solubility of hafnium in the nickel matrix of a laser-clad Ni–Cr–Al–Hf–Re alloy. This was determined by parallel experiments conducted on the binary Ni–Hf system. Elemental powders of nickel and hafnium were mixed in the ratio of 74 wt% Ni and 26 wt%Hf. The clad alloys were made under identical laser processing conditions [34]. Fig. 33 is a transmission electron micrograph of a section of secondary dendrite arms showing the circular and ellipsoidal morphology of the alpha (α) phase. During the formation of α-phase, solute (hafnium in excess of the amount that can be trapped within the α phase (due to rapid cooling) is rejected towards the periphery of the dendritic arms. The excess hafnium, together with the remaining liquid, forms a eutectic transformation product, *E*. Some undissolved or partially dissolved particles were trapped in the laser-clad alloy (indicated by arrows) due to its high melting point and rapid solidification. A dedicated scanning transmission electron microscope (Vacuum Generator HB-501) was employed to establish the solid solubility of hafnium present in the various phases (Fig. 33). Table II shows the microchemistry of Ni–Hf alloys [34].

The maximum solid solubility of hafnium in the α-phase under laser-clad conditions was about 11–13 wt%, which is much higher than under equilibrium conditions. In addition, a non-equilibrium eutectic structure was observed in the laser-clad Ni–Hf system [34]. The eutectic phase mixture consists of δ_E (hafnium-rich) and α_E (hafnium-lean) phases. The δ_E phase is a non-equilibrium (unreported) phase. The TEM–convergent-beam microdiffraction technique was employed to determine the crystal structure of non-equilibrium phase (Fig. 34) and had a tetragonal crystal structure [34]. Based on microstructure and microchemistry of the phases developed in the laser-clad Ni–Hf alloy, a non-equilibrium phase diagram was established (Fig. 35). Thus, a possible phase-transformation sequence could be suggested based on microstructural evolutions.

$$L \rightarrow + L \rightarrow \alpha + E = \alpha + (\alpha_E + \delta_E) \quad (10)$$

where E represents the eutectic mixture of $(\alpha_E + \delta_E)$.

6.3.4. Wear-resistant coatings

Laser cladding was found be very useful for developing a wear-resistant coating on less expensive materials. Singh and Mazumder have undertaken extensive work on *in situ* formation of complex carbides of Fe–Cr–X–C (X = W, Mn, Mo) alloys in plain carbon steel [36–39]. The hardness profile between the laser-clad region of Fe–Cr-Mn–C alloy and the substrate is presented in Fig. 36. The top section of the laser-clad region has a high hardness value (~ 675 VHN) while the average hardness value of the clad region is ~ 550 VHN. The hardness scatter is due to the presence of a very fine duplex microstructure in the clad region consisting of carbide precipitates, metastable phases, and the matrix phase.

Preliminary wear data for laser-clad samples as a function of laser power and traverse speed are given in Fig. 37. For comparison, wear and coefficient of friction data of base material and Stellite-6 are also presented. Note that the wear data are presented in terms of "width of the wear scar". If the data were plotted in terms of wear volume, there would be a more dramatic difference between the laser-clad surface and Stellite-6. This suggests that the surface properties of the base materials can be easily improved by laser cladding. Scanning electron microscopy (SEM) examination of the laser clad Fe–Cr–W–C alloy shows a uniform distribution of tungsten carbide precipitate in the matrix (Fig. 38). In order to determine the distribution of alloying elements throughout the clad region, electron probe microanalysis (EPMA) was carried out and the results are shown in Fig. 39. There is uniform distribution of tungsten carbide in the clad region. The average distribution of tungsten in the form of carbide is about 8 wt %, whereas the distribution of chromium and iron vary in a complementary fashion (i.e. wherever a peak of chromium in the clad region occurs, there is a corresponding depletion of iron). This could be due to variation in the composition of carbides and matrix. In addition, near the clad/matrix interface, there are equal concentrations of chromium and iron and the concentrations of chromium and tungsten go to zero.

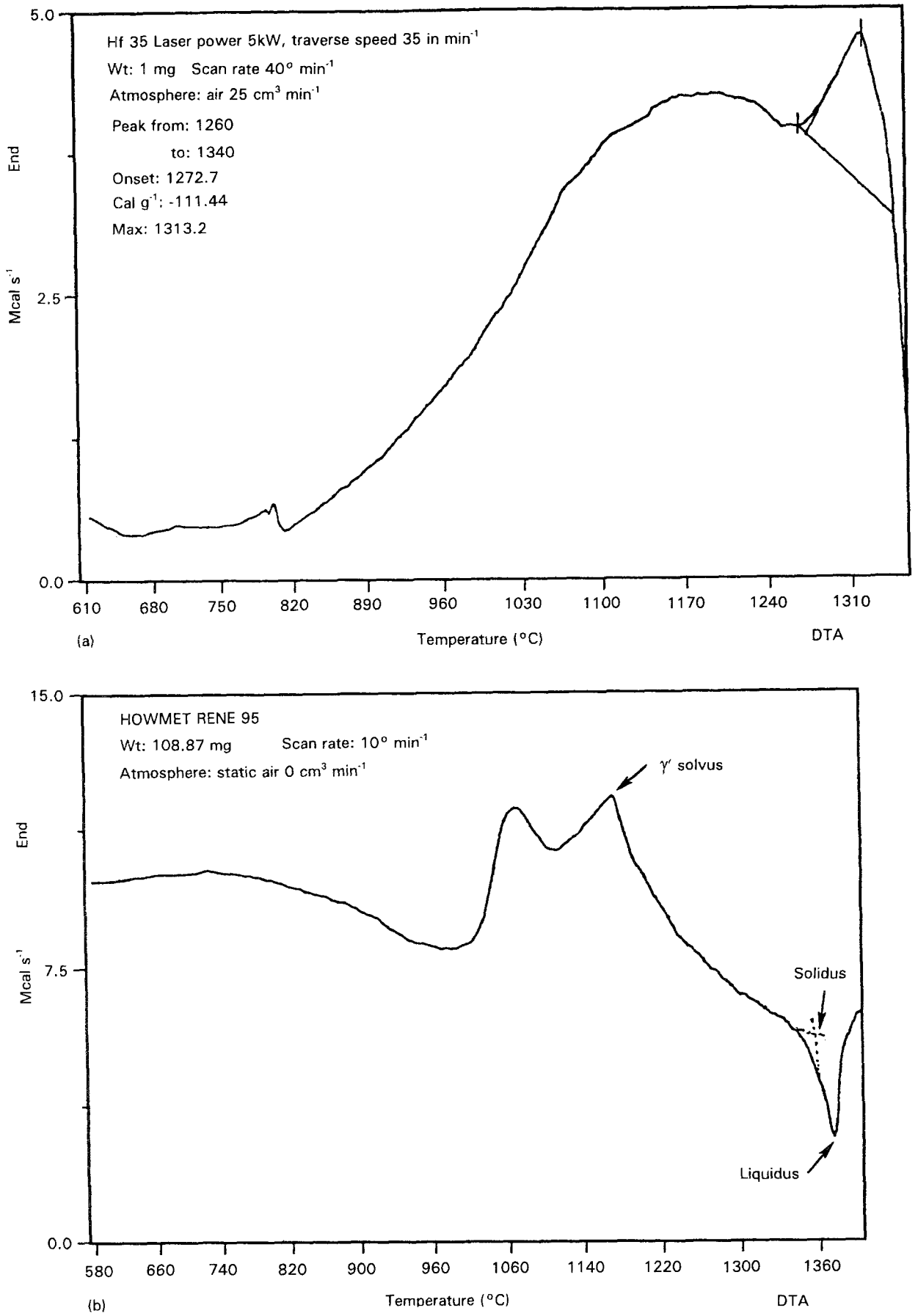

Figure 30 A plot of differential thermal analysis (DTA) of (a) the laser-clad alloy and (b) Rene 95.

The laser-clad zone can be divided into two parts. The upper zone is rich in alloying elements and has a uniform microstructure as discussed above. The lower zone is rich in base material (i.e. the substrate). This part of the laser-clad region exhibited columnar growth as shown in Fig. 38 and corresponds to equal concentrations of iron and chromium near the interface (Fig. 39).

Looking more closely at the laser clad/substrate interface, solidification first occurred by the formation

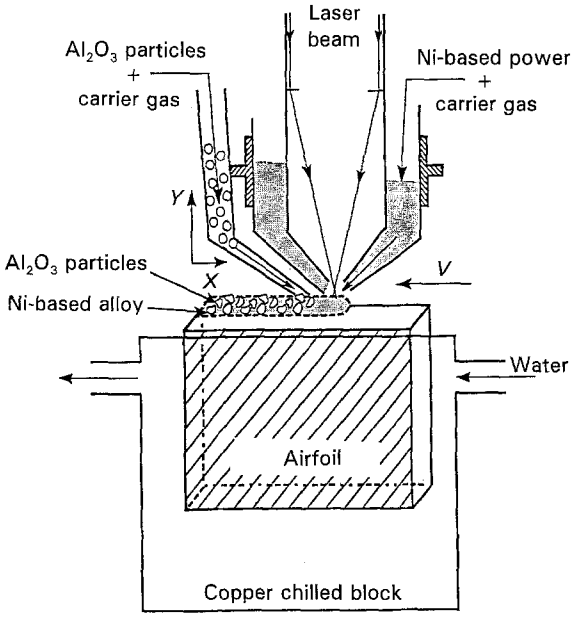

Figure 31 A schematic diagram showing the side delivery of abrasive powder particles (Al_2O_3) into the melt-pool region of the substrate.

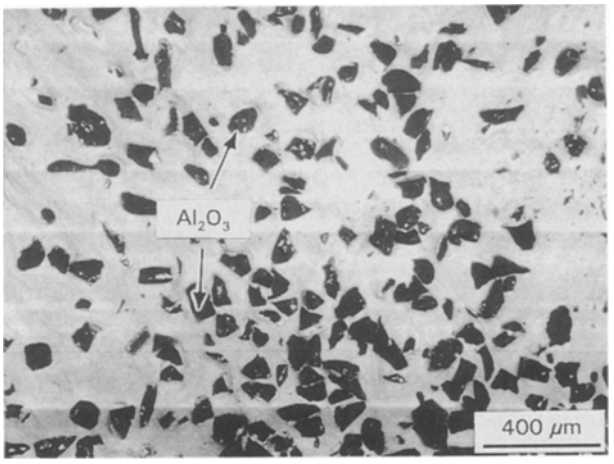

Figure 32 Scanning electron micrograph showing the entrapped ceramic Al_2O_3 particles in the surface of laser-clad Ni–Cr–Al–Hf alloy.

of dendrites from the substrate. The dendrites are rich in iron, containing relatively small amounts of chromium and, perhaps, no carbon. The growth distance of the dendrites is about 10 μm, and this depends upon the laser energy input, rate of solidification, and amount of undercooling. This can be explained using a heat and mass transfer model proposed by Li and Mazumder [41]. In the case of powder delivered directly at the beam interaction region, the specific energy of the laser beam is consumed by simultaneous melting of the powder and the substrate. Because of the unique fluid-flow mechanism, the melt-pool region is a homogeneous liquid solution.

During solidification, the latent heat energy would be evolved and is conducted to the substrate. This latent heat energy melts an additional layer of the substrate but there is not enough time to remix with the remaining melt. Thus, the banded zone is rich in

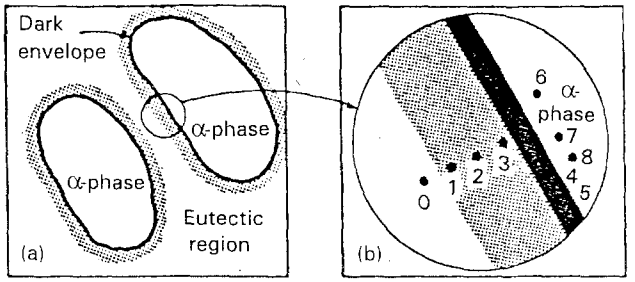

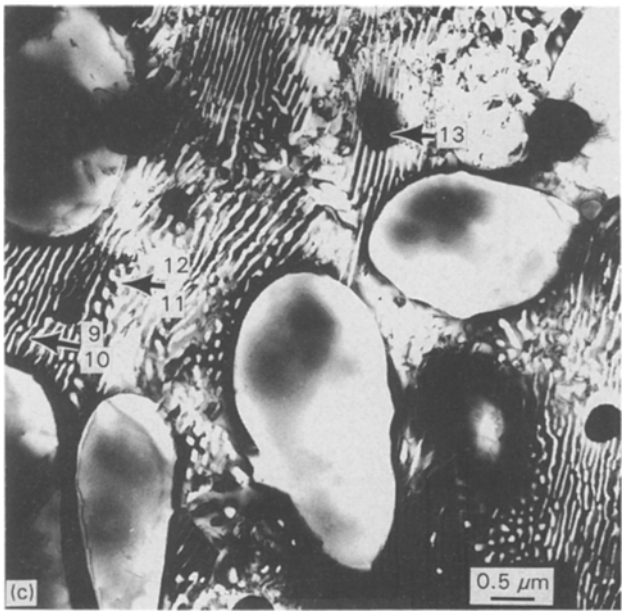

Figure 33 STEM micrograph of the laser-clad Ni–Hf alloy showing the X phase and eutectic phase. Inset is a schematic diagram showing the positions of the probe from where microanalysis was performed.

TABLE II Microchemistry studies of Ni–Hf alloys [34]

Probe position	Comments	(wt%)		(at %)	
		Ni	Hf	Ni	Hf
0	See Fig. 33	45.1	54.9	71.4	28.6
1	See Fig. 33	44.0	56.0	70.5	29.5
2	See Fig. 33	48.1	51.9	73.8	26.2
3	See Fig. 33	63.7	36.3	84.2	15.8
4	See Fig. 33	72.8	2.72	89.1	10.9
5	See Fig. 33	72.2	27.8	89.8	11.2
6	See Fig. 33	88.1	11.9	95.7	4.3
7	See Fig. 33	86.8	13.2	95.2	4.8
8	See Fig. 33	87.3	12.7	95.4	4.6
9	Dark area	48.3	51.7	73.9	26.1
10	of eutectic	49.2	50.8	74.7	25.3
11	Bright area	83.7	16.3	93.9	6.1
12	of eutectic	83.8	16.1	93.9	6.1
13	Partially dissolved Hf (hexagonal)	19.6	80.4	42.6	57.4

the substrate (iron) phase. Away from the substrate/cladding interface and towards the top of the clad region, because of high mixing, the substrate is almost uniform with little dilution. Similar findings have been observed in other clad materials such as Mg–Al, Fe–Cr–Mn–C, and nickel-based alloys [30].

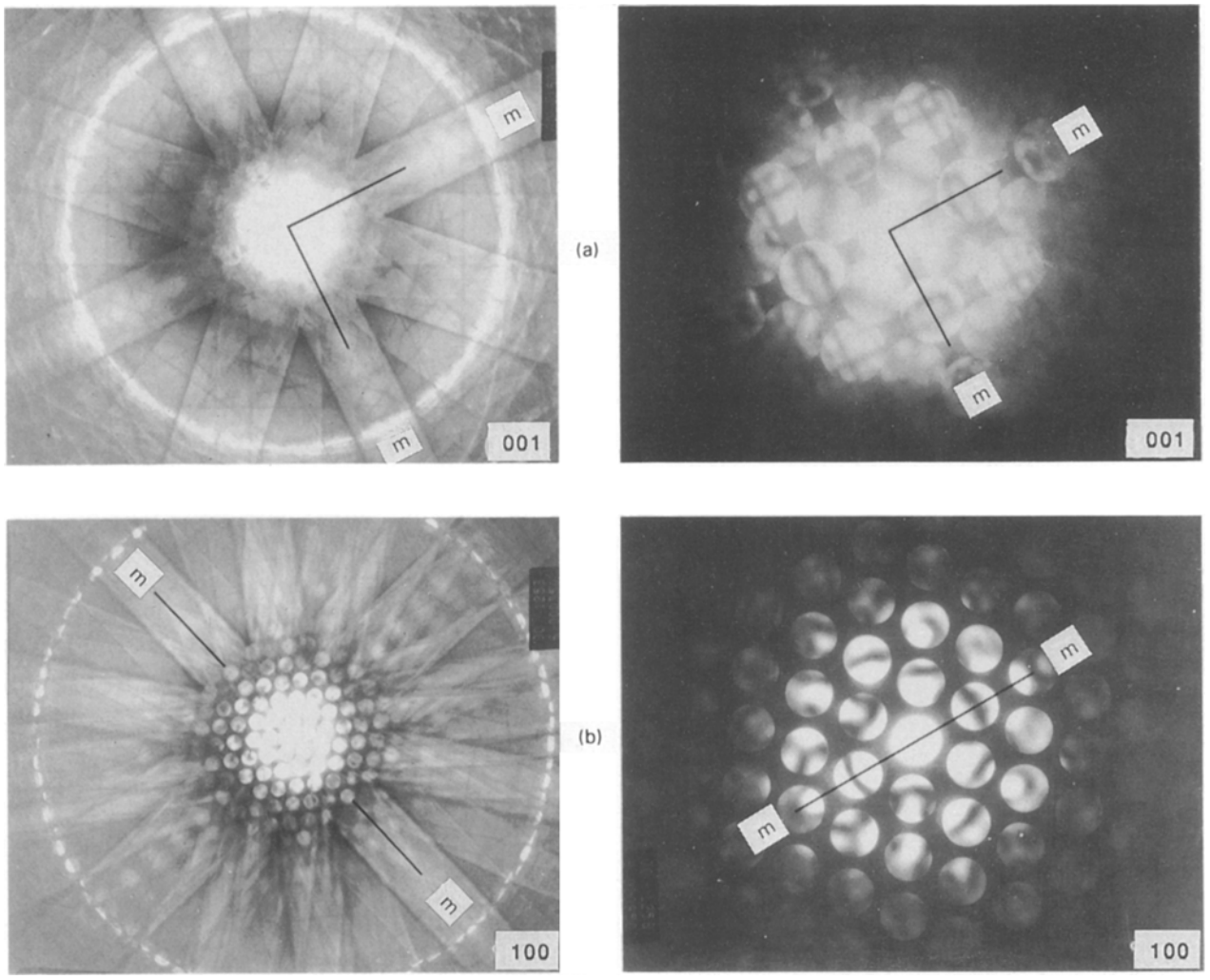

Figure 34 TEM– convergent beam microdiffraction patterns taken from the δ_E phase. (a) [001] showing 4 mm whole pattern and zero-order zone symmetries, (b) [100] showing m whole pattern and zero-order zone symmetries [34].

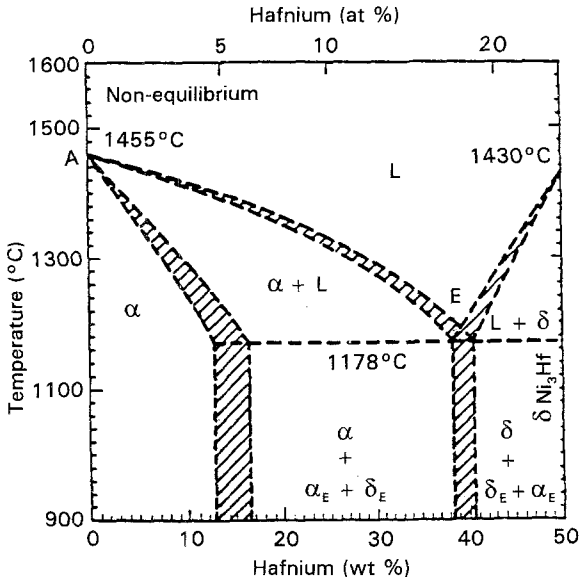

Figure 35 The non-equilibrium phase diagram of the Ni–Hf system up to ~ 50 wt% Hf.

6.3.5. Corrosion-resistant coatings

Magnesium-based alloys have recently attracted considerable attention from the aircraft industry because they are light in weight and have good mechanical properties. However, magnesium alloys also have poor corrosion resistance. Resistance can be improved by laser cladding magnesium with pure zirconium. Magnesium melts at about 650 °C and has a density of 1.74 g cm^{-3}, whereas zirconium has a melting point of 2050 °C and a density of 6.49 g cm^{-3}. In addition, magnesium evaporates before zirconium melts, thus making an alloy of the two elements is difficult. From the available phase diagram of Mg–Zr, the maximum solid solubility of zirconium in the magnesium is 0.6 wt%. Unfortunately, a phase diagram of zirconium-rich Mg–Zr is not available [42].

For laser cladding, zirconium powder was placed on a magnesium sample and a laser beam was scanned on the powder under an argon atmosphere. The zirconium rapidly melted and the magnesium partially melted. While molten, the two metals attempted to mix but, because of the rapid melting and solidification, there was poor mixing. Fig. 40 shows the microstructure of a section of a zirconium-clad magnesium alloy. The clad region is divided into two parts, labelled A and B in Fig. 40. The upper portion of the clad region (A) consists of 100% Zr. The concentration of zirconium decreased towards the magnesium substrate until region B where a mechanical mixture of zirconium and magnesium occurred. EPMA was carried out across the clad region and substrate. Fig. 41 revealed that the top section (region

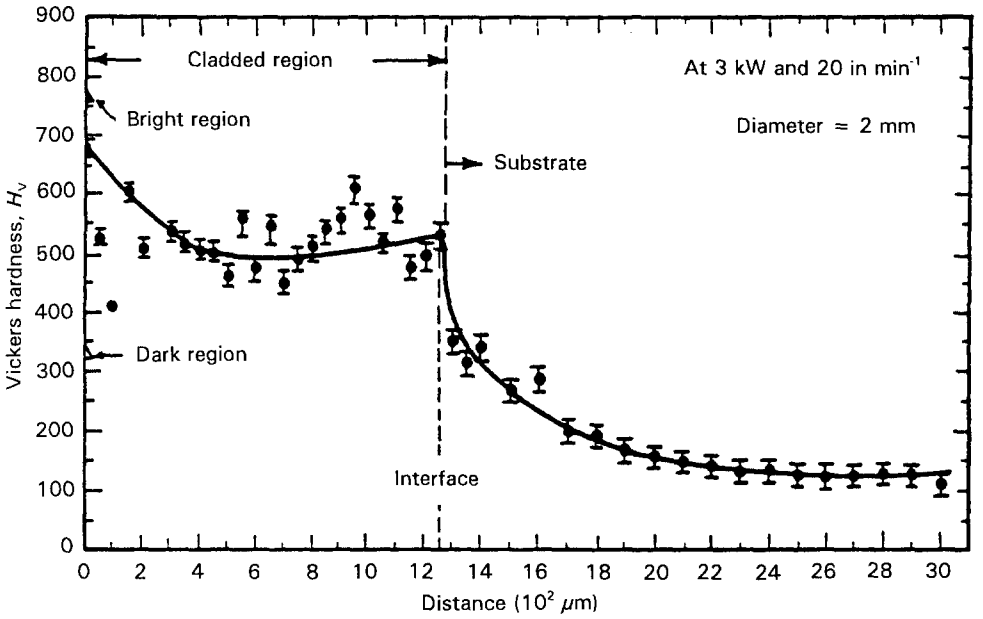

Figure 36 Hardness variation in the laser-clad Fe–Cr–Mn–C alloy.

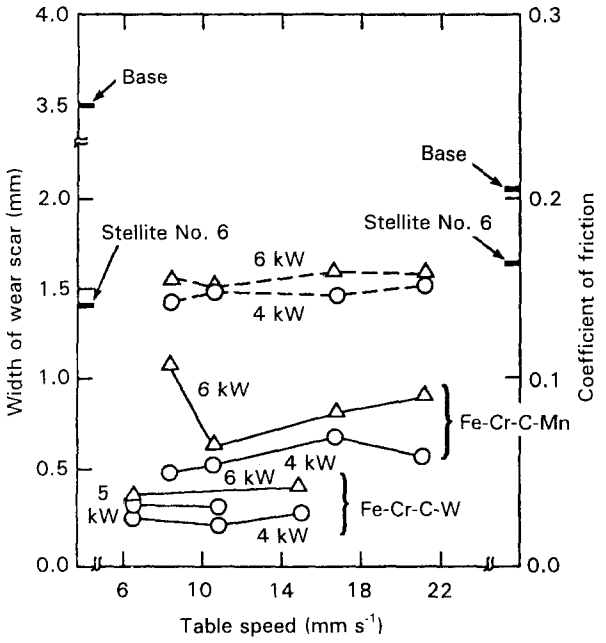

Figure 37 (– – –) Friction and (———) wear of laser-clad alloys as a function of traverse speed and laser power [39, 40].

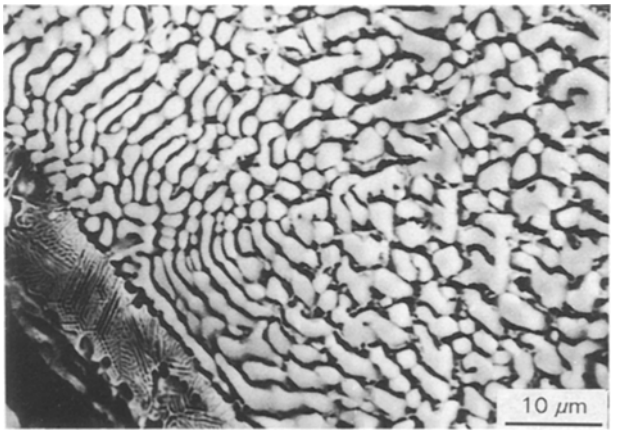

Figure 38 Scanning electron micrograph of the laser-clad Fe–Cr–W–C alloy showing uniform distribution of tungsten carbide precipitate.

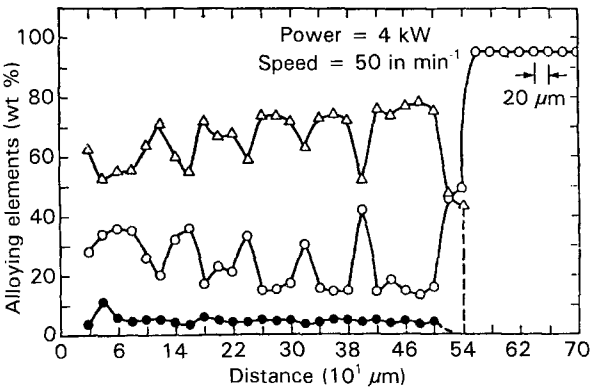

Figure 39 EPMA of the laser-clad Fe–Cr–W–C alloy showing distribution of alloying elements across the laser-clad region and substrate. (△) Cr, (○) Fe, (●) W.

A) was 100% Zr. In region B, the concentration of both zirconium and magnesium varied from 0% –100%, indicating a mechanical mixture of zirconium and magnesium. Below the interface region, the content of zirconium dropped to zero.

STEM was carried out for microstructural examination of the laser Zr–Mg clad alloy. Formation of an amorphous phase was observed in region A of Fig. 42a. The selected-area diffraction (SAD) pattern from region A of Fig. 42a shows diffuse rings (Fig. 42b), while region C has a crystalline structure, and region B shows a duplex structure of amorphous plus crystalline regions. Fig. 42c is an SAD pattern at the amorphous/crystalline interface (clearly visible in Fig. 42a), showing both diffuse rings from the amorphous region A and sharp spots from crystalline region C. Table III, which shows a semi-qualitative microanalysis of regions A, B and C reveals that region A is rich in zirconium, whereas the crystalline region was relatively low in zirconium. This is the first known

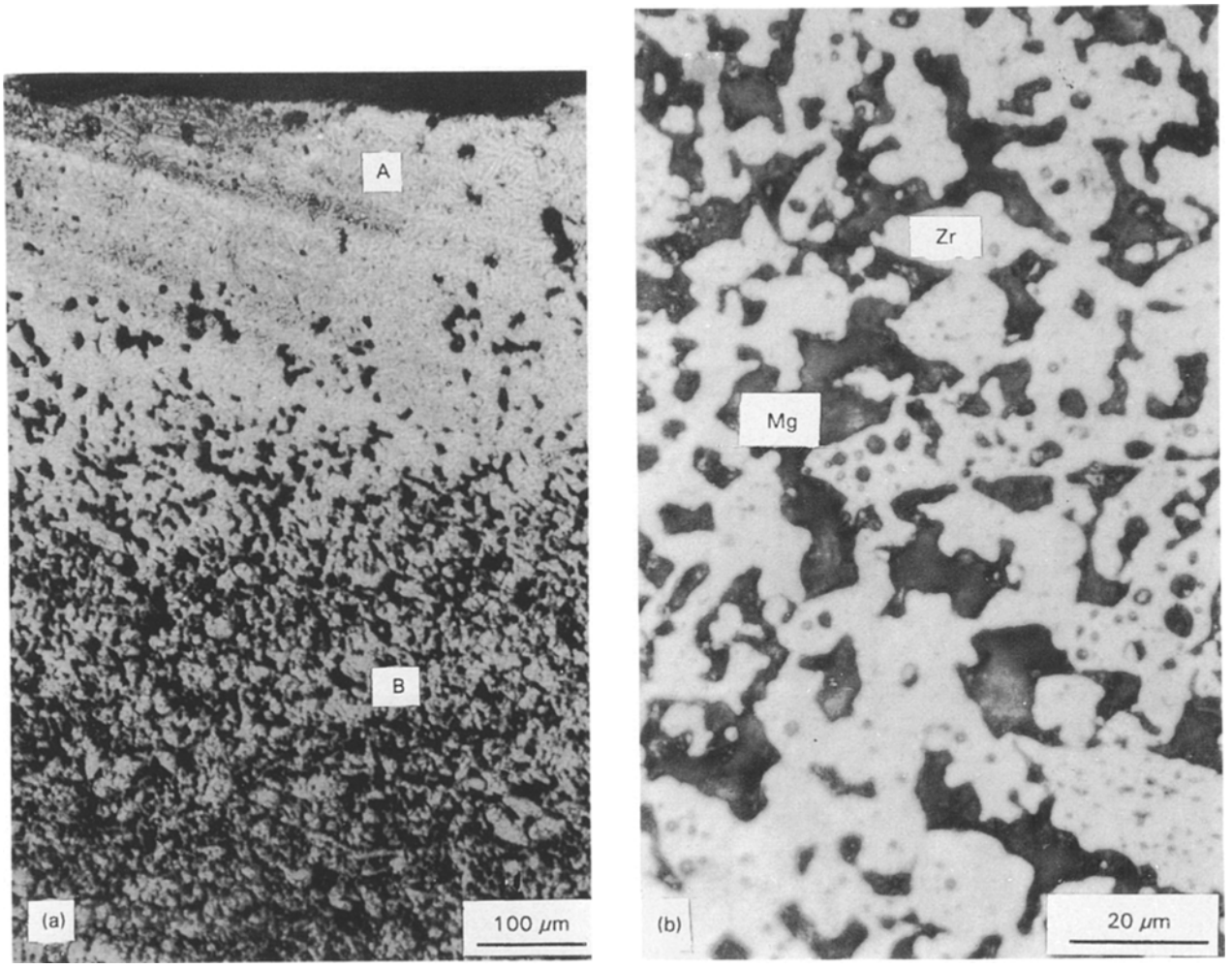

Figure 40 (a, b) Optical micrographs showing the laser cladding of zirconium on magnesium substrate.

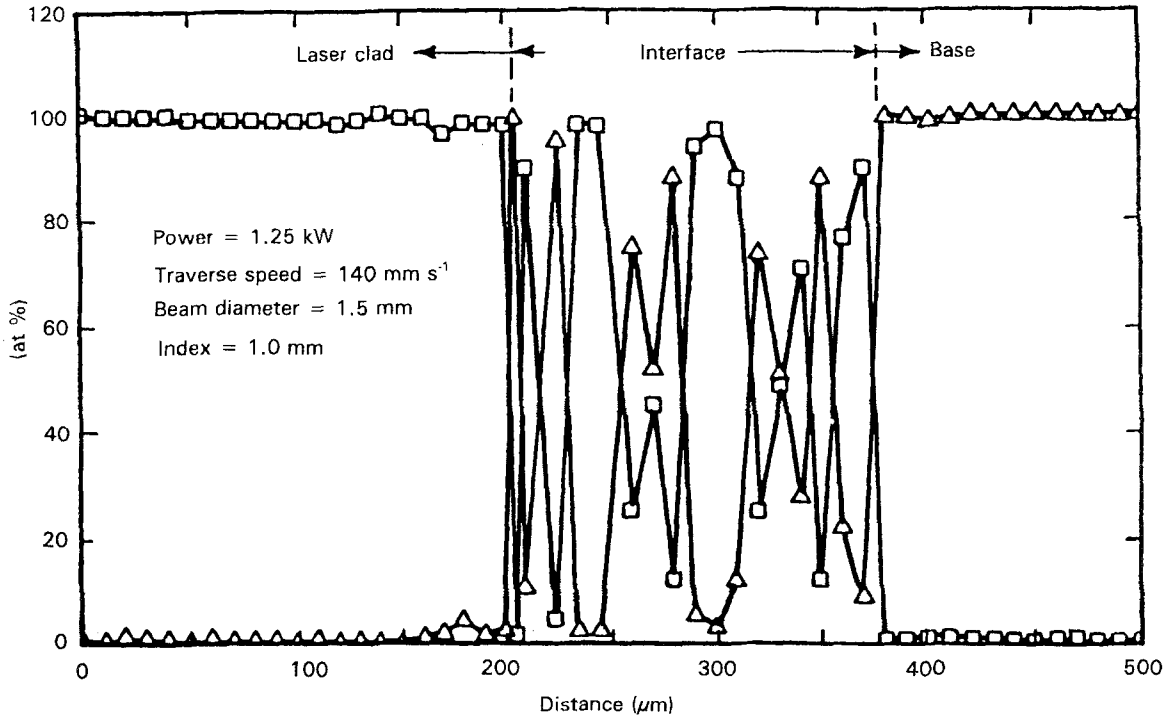

Figure 41 EPMA of the laser-clad Zr–Mg alloy showing the distribution of each of the alloying elements across the clad and substrate. (□) Zr cladding, (△) Mg base.

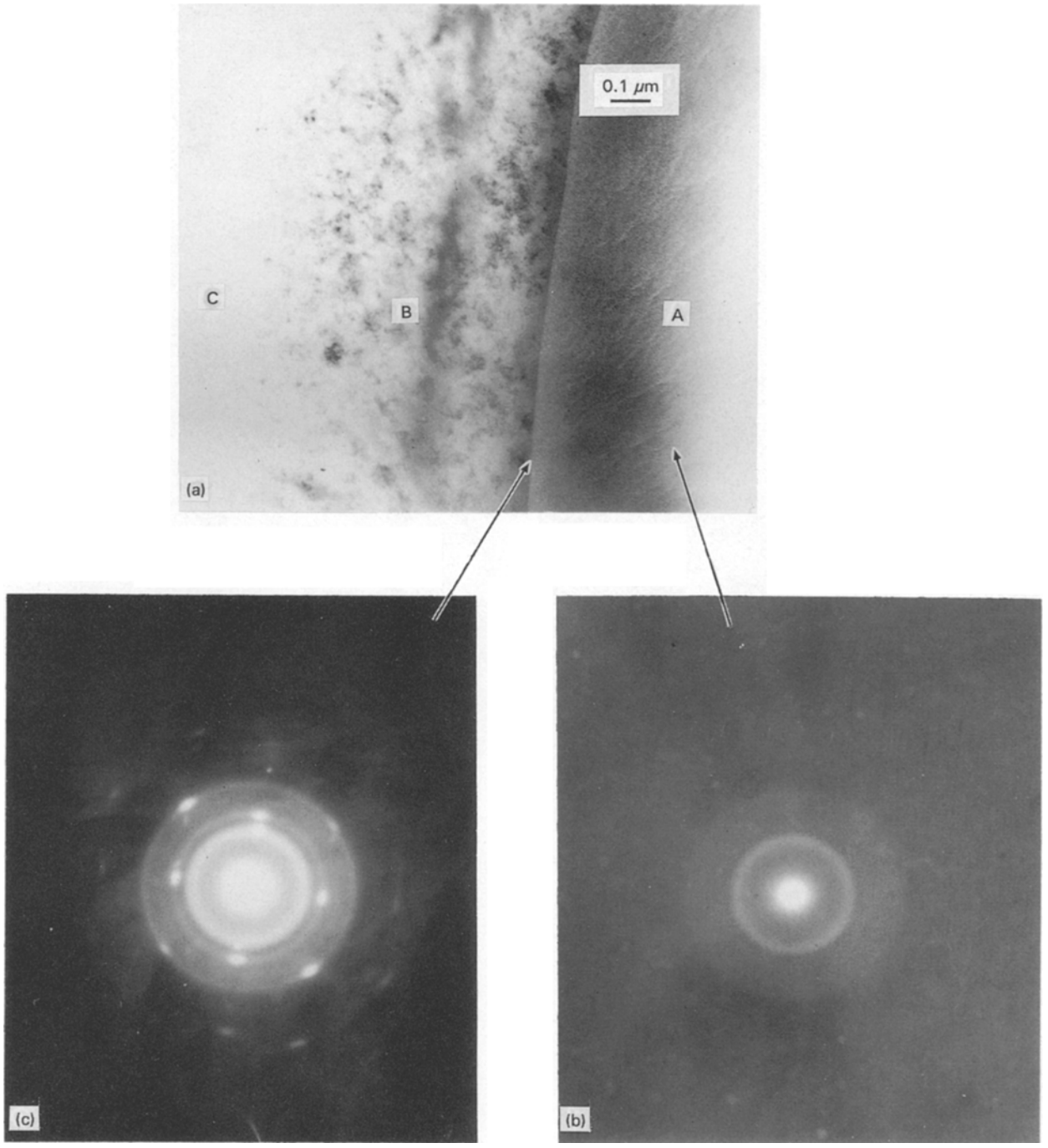

Figure 42 TEM analysis of laser-clad Mg–Zr alloy showing the existence of an amorphous phase in this system: (a) bright-field micrograph showing the amorphous phase (A), interface, crystalline region (B and C); (b) diffused ring; (c) SAD pattern near the interface showing both diffused rings and diffracted spots from region B or C.

TABLE III Composition of amorphous and crystalline region of Fig. 42

Region	Composition (wt%)	
	Mg	Zr
Amorphous (A)	15.4	84.6
Interface	49.4	50.6
Crystalline (B and C)	74.5	25.5

report of amorphous phase formation in the zirconium-rich Mg–Zr system.

The clad region also shows the existence of a martensitic structure due to phase transformation in the zirconium-rich portion. Table IV evaluates the corrosion properties of laser cladding zirconium on magnesium and other clad alloys for comparison.

6.4. Surface hardening

Surface hardening is used to improve wear resistance and fatigue strength. Localized annealing and transformation hardening of cast iron and iron-based alloys are the typical examples of surface hardening. The interaction of the high-energy laser beam with the substrate generates localized heat at the surface. The temperature of the finite volume of the substrate is rapidly increased to austenitizing temperature which,

TABLE IV Corrosion properties of various materials

Material	Corrosion potential in 3.5% NaCl
Mg (laser clad with Zr)	− 0.647
Al (cold rolled)	− 0.674
Al (powder compact)	− 0.733
Al (laser clad)	− 1.335
Mg (as received)	− 1.526
Mg alloy	− 1.455

on rapid cooling (self-quenching), transforms to martensite. In such a process, most of the heat is transferred through the substrate by heat conduction. Because the transformation hardening occurs only at the surface, the power of the laser beam is confined to prevent surface melting. The volume fraction of surface hardening depends on the laser processing conditions. Ganamuthan [16], Li *et al.* [17] and Abboud and West [18] have performed impressive theoretical modelling and experimental work on the laser heat treatment of low-alloy steels and cast iron.

6.5. Shock hardening

A pulsed laser beam with a nominal power density of 10 GW cm^{-2} and pulse duration of 20–40 ns can rapidly vapourize a thin surface layer (a few atomic layers) of the work piece. During removal of the surface atoms, a momentum impulse takes place and generates a shock wave or stress wave. The effect of the high-power laser pulse is primarily mechanical and is localized to a region near the irradiated surface. In such treatments the thermal effects are negligible. A Q-switched YAG laser was used in shock hardening of cast iron and 7075 and 7475 aluminium alloys. The magnitude of the shock wave was 5.6 GPa. There was an increase in the fatigue life of both the aluminium alloys which was attributed to the presence of residual compressive stresses as the surface [14].

6.6 Cutting

The laser has gained substantial confidence in the metal-cutting industries. Two types of laser are commonly used in the cutting industries namely the CO_2 and the YAG. The high-power CO_2 laser has more potential applications in the metal-cutting industries compared to the YAG laser, which is limited to low-power level and a much slower cutting speed (about five times) compared with the CO_2 laser (cutting speed) 120–150 in min^{-1}; ~ 305–380 cm min^{-1}). The CO_2 laser can be used as CW or pulse mode. The high-power laser beam can be assisted with the mixture of gases (argon, helium, nitrogen, etc.) at various gas pressures. If the gas pressure is more than 120 p.s.i. (10^3 p.s.i. = 6.89 N mm^{-2}) then the cutting process is called "clean cut". The function of a high-pressure gas mixture with the laser beam on the target, is to remove rapidly the molten material from the surface and to provide a high rate of cooling to the cut surface [43]. In addition, it acts as a shielding gas. The "clean cut" process will provide a smooth and clean surface free from draws and recast layer. In addition, it will also minimize the heat-affected zone (HAZ) developed in the metal during the cutting operation. The width of the HAZ depends upon the laser processing parameters, i.e. laser power (energy), traverse speed (interaction time), pressure of gas mixture, laser beam diameter, thickness of material to be cut. The main metallurgical concern is the HAZ developed in materials even after the laser "clean cut" process. It is well documented in the literature that titanium alloys are more sensitive to HAZ compared with other alloys such as Inconel, A286 steel, aluminium alloys, and stainless steels.

Abrasive water jet (AWJ) is a relatively new technology which is competing with laser in cutting industries such composite, ceramic, leather, etc. [43]. The significance of this process is that it is a cold process and does not generate HAZ. Typical cutting speeds are 10–30 in min^{-1} (25.4–76.2 cm min^{-1}). However, the main metallurgical concerns in the AWJ-cut materials are impingement of the abrasive particles into the matrix, grain-boundary tearing, mechanical-groves formation, intergranular cracks and residual stresses. All these factors have an impact on the mechanical properties of material. Thus, the laser still has a leading edge in the metal-cutting industries [43].

7. Conclusion

A laser can perform different functions by manipulating the laser-processing conditions such as energy, beam diameter, interaction time, etc. Lasers have been successfully used in many applications, such as drilling, cutting, welding, laser glazing, cladding, and heat treatment. Even new engineering materials have been economically tailored on low-cost work pieces to meet specific requirements, e.g. wear-corrosion- and oxidation-resistant surfaces.

The laser has also been successfully used in the electronic industries. LAPVD and LACVD processes have been used to synthesize new materials and high-quality thin films which are highly desirable for fabricating microchips. These processes are still in the infant stage and are being explored in other areas.

References

1. J. CHEUNG and J. HORWITZ, *MRS Bull.* **2** (1993) 30.
2. F. BEECH and I. W. BOYD, "Photochemical Processing of Electronic Materials", edited by I. W. Boyd and R. B. Jackman (Academic Press, New York, 1991) pp. 387–429.
3. J. E. READY, "Effect of High Power Radiation" (Academy Press, New York, 1971).
4. R. SINGH and J. NARAYAN, *Phys. Rev.* **B 41** (1990) 8843.
5. S. M. SHIN, C. W. DRAPER, M. E. MOCHEL and J. M. RIGSBEE, *Mater. Lett.* **3** (1985) 265.
6. X. BI, B. GANGULY, G. P. HUFFMANS, F. E. HUGGINS, M. ENDO, and P. C. EKLUND, *J. Mater. Res.* **8** (1993) 1666.
7. P. A. MOLIAN and A. WASCHEK, *J. Mater. Sci.* **28** (1993) 1733.
8. S. B. OGALE, *Phys. Rev.* **B36** (1987) 8237.
9. J. SINGH and M. VELLAIKAL, *J. Appl. Phys.* **73** (1993) 2831.

10. J. SINGH and M. VELLAIKAL, in Proceedings of the "International Conference on Beam Processing of Advanced Materials", edited by J. Singh and S. M. Copley (TMS, Chicago, IL 1992) p. 383.
11. W. M. STEEN and J. N. KAMALU, in "Laser Materials Processing", edited by M. Bass (North-Holland, Amsterdam, 1983) p. 83.
12. M. MORI and H. KUMEHARA, *Bull. Jpn. Soc. Precision Eng.* **10** (1976) 1773.
13. J. MAZUMDER, *J. Metals* **35** (5) (1983) 19.
14. C. L. CHAN, PhD thesis, University of Illinois, Urbana, IL (1986).
15. J. C. ION and K. E. EASTERLING and M. F. ASHBY, *Acta Metall.* **32** (1984) 1949.
16. D. S. GANAMUTHAN, in "Application of Laser in Materials Processing", edited by E. A. Metzbower (ASR, Materials Park, OH, 1979) p.22.
17. W. B. LI, K. E. EASTERLING and M. F. ASHBY, *Acta Metall.* **32** (1986) 1533.
18. J. H. ABBOUD and D. R. F. WEST, *J. Mater. Sci.* (1992) 1479.
19. STEFAN JOHANSON, *et al., J. Appl. Phys.* **72** (1992) 5956.
20. C. W. DRAPER and J. M. POATE, *Int. Mater. Rev.* **30** (2) (1985) 85.
21. N. IWAMOTO, *Surf. Coat. Technol.*. **34** (1988) 59.
22. C. ORTIZ and K. A. RUBIN, *J. Mater. Res.* **3** (1988) 1196.
23. B. C. OBERLANDER and E. LUGSCHEIDER, *Mater. Sci. Technol.* **8** (1992) 657.
24. F. H. SCOTT, P. K. N. BARTLETT, and G. C. WOOD, *Oxid. Metals* **27** (112) (1987) 37.
25. J. SINGH, B. N. BHAT, R. POORMAN, A. KAR and J. MAZUMDER, *Coat. Surf. Technol.* (1994) submitted.
26. J. SINGH, G. JERMAN, R. POORMAN and B. N. BHAT, NASA Technical Report 108419 (1993).
27. J. SINGH, R. POORMAN and B. N. BHAT, NASA Technical Report 108431 (1993).
28. J. SINGH and J. MAZUMDER, *Acta Metall.* **35** (1987) 1987.
29. J. SINGH and K. NAGANATHAN and J. MAZUMDER, *High Temp. Technol.* **5** (3) (1987) 131.
30. J. SINGH and J. MAZUMDER, *Metall. Trans.* **8** (1988) 1588.
31. R. D. RAWLINGS and A. S. BEVAN, *J. Mater. Sci.* **10** (1975) 505.
32. J. R. NICHOLLS, PhD thesis, London University (1974).
33. A. BALDAN, *Z. Metallkde* **1** (1985) 24.
34. S. SARKAR, J. SINGH and J. MAZUMDER, *Acta Metall.* **37** (1989) 1167.
35. D. S. GNANAMUTHAN, in "Application of Laser in Materials Processing", edited by E. A. Metzbower (ASM, Materials Park, OH, 1979) p. 22.
36. J. SINGH and J. MAZUMDER, *Metall. Trans.* **18** (1987) 313.
37. *Idem, J. Mater. Sci. Technol.* **2** (1986) 709.
38. *Idem*, in "Proceedings of International Conference on Applications of Laser and Electron Optics", edited by J. Singh and J. Mazumder (Laser Institute of America, Orlando, FL, 1986) p. 539.
39. *Idem*, "Microstructure and Wear Properties of Laser Clad Fe–Cr–Mn–C Alloy", Report No. 127 (University of Illinois, Urbana, IL, 1987).
40. L. J. LI and J. MAZUMDER, in "Laser Processing of Materials", edited by K. Mukherjee and J. Mazumder TMS, Warrendale, PA, 1984) p. 35.
41. E. EIHOLZER, C. CUSANO and J. MAZUMDER, *ICALEO* **34** (1985) 1840.
42. J. SINGH, *J. Metals* **9** (1992) 8.
43. J. SINGH and S. C. JAIN, *J. Mater. Sci.* (1994) submitted.
44. J. NARAYAN, P. TIWARI, X. CHEN, J. SINGH, R. CHOWDHURY and T. ZHELEVA, *Appl. Phys. Lett.* **61** (1992) 1290.

Received 22 December 1993
and accepted 14 February 1994